

**NASA Technical Memorandum 104566, Vol. 10**

## **SeaWiFS Technical Report Series**

**Stanford B. Hooker, Editor**  
*NASA Goddard Space Flight Center*  
*Greenbelt, Maryland*

**Elaine R. Firestone, Technical Editor**  
*General Sciences Corporation*  
*Laurel, Maryland*

## **Volume 10, Modeling of the SeaWiFS Solar and Lunar Observations**

**Robert H. Woodward**  
*General Sciences Corporation*  
*Laurel, Maryland*

**Robert A. Barnes**  
*CHEMAL, Inc.*  
*Wallops Island, Virginia*

**Charles R. McClain, Wayne E. Esaias,  
William L. Barnes, and Ann T. Mecherikunnel**  
*NASA Goddard Space Flight Center*  
*Greenbelt, Maryland*



National Aeronautics and  
Space Administration

**Goddard Space Flight Center**  
Greenbelt, Maryland 20771

## ABSTRACT

Post-launch stability monitoring of the Sea-viewing Wide Field-of-view Sensor (SeaWiFS) will include periodic sweeps of both an onboard solar diffuser plate and the moon. The diffuser views will provide short-term checks and the lunar views will monitor long-term trends in the instrument's radiometric stability. Models of the expected sensor response to these observations were created on the SeaWiFS computer at the National Aeronautics and Space Administration's (NASA) Goddard Space Flight Center (GSFC) using the Interactive Data Language (IDL) utility with a graphical user interface (GUI). The solar model uses the area of intersecting circles to simulate the ramping of sensor response while viewing the diffuser. This model is compared with preflight laboratory scans of the solar diffuser. The lunar model reads a high resolution lunar image as input. The observations of the moon are simulated with a bright target recovery algorithm that includes ramping and ringing functions. Tests using the lunar model indicate that the integrated radiance of the entire lunar surface provides a more stable quantity than the mean of radiances from centralized pixels. The lunar model is compared to ground-based scans by the SeaWiFS instrument of a full moon in December 1992. Quality assurance and trend analyses routines for calibration and for telemetry data are also discussed.

## 1. INTRODUCTION

This document describes analytical prototypes for post-launch lunar and solar diffuser observations, plus quality control and trend analysis routines for data related to instrument calibrations and engineering. The lunar and solar diffuser observations do not provide an absolute calibration traceable to National Institute of Standards and Technology (NIST) standards and are correctly viewed only as stability checks. However, they are closely coupled to an understanding of the temporal changes in instrument calibration relative to the sun, and thus the terms "calibration" and "observations" are nearly synonymous.

All the software routines were developed on the Sea-viewing Wide Field-of-view Sensor (SeaWiFS) Calibration/Validation (CALVAL) SGI 440 workstation. It is expected that these modeling tasks will add to the understanding of the calibration operations as well as to the understanding of potential problems. Many of the routines developed for this task may either be directly ported to the SeaWiFS operational environment or may provide the groundwork for future software development.

The observation models and simulated input data are designed to be as realistic as possible. Solar irradiances are integrated to the SeaWiFS bands and are read as input for both the diffuser and lunar models. A high resolution lunar image is also read as input in the lunar model. Laboratory simulations of the diffuser observations are compared to the solar model, and ground-based lunar scans by the SeaWiFS instrument are compared to the lunar model.

Most of the software routines discussed in this document were implemented using the Interactive Data Language (IDL) software package. This utility is an interpreted/compiled language which is designed for statistical analysis and display of large multidimensional arrays or images. IDL is used for the calibration task since much of

the data related to this task will be ingested and analyzed as images. IDL also provides a graphical user interface (GUI) allowing easy manipulation of models.

## 2.0 ONBOARD CALIBRATIONS

Lunar and solar on-orbit measurements are intended for the monitoring of changes in the radiometric sensitivity of the SeaWiFS instrument. These measurements will complement interchannel gain and time delay integration (TDI) checks, which also track changes in the sensor. For solar measurements, the instrument has two diffuser surfaces—the solar flight diffuser and a nearly identical surface on the back of the solar flight diffuser cover. The sequence of measurements will include the monitoring of changes in the reflectance of the diffuser cover and the exposure of the flight diffuser with the removal of the cover. Early in the mission, there will be more calibrations to provide an accurate baseline for further assessment.

Many of the onboard calibration related activities will occur while the platform is over the South Pole or in back-orbit, minimizing interference with ocean data collection. Lunar measurements will involve scanning the moon at 1–3 month intervals when the moon is within 7° of full. The solar diffuser will be scanned at shorter intervals between lunar measurements to provide complete temporal coverage.

It is expected that the diffuser will degrade with time as contaminants condense on the surface. In contrast, the lunar surface is assumed to maintain stable reflective properties. Lunar observations will therefore provide anchor points for calculating trends in the calibrations. The calibration and instrument telemetry data will undergo quality control and time series analyses prior to being stored in the CALVAL archive. These analyses will include screening for outliers and discerning trends in the measurements.

For a complete description of the calibration activities see McClain et al. (1992).

## 2.1 Calibration Background

Lunar measurements are the single source of information for monitoring the long-term drift in the radiometric sensitivity of the SeaWiFS instrument. The sun and the surface of the moon are considered as stable, non-changing light sources. Variations can be accounted for in the incident solar flux due to changes in the Earth-sun distance by using (Gordon et al. 1983):

$$F_0 = \bar{F}_0 \left[ 1 + e \cos \frac{2\pi(D-3)}{365} \right]^2 \quad (1)$$

where  $D$  is the sequential day of the year,  $e$  is orbit eccentricity (0.016), and  $\bar{F}_0$  is the mean solar irradiance. In a similar manner, variations in the reflectance of the moon, due to small differences in the lunar phase angle and due to small changes resulting from lunar libration, can also be removed by calculation. With these corrections, changes in measurements of the lunar reflectance can be used directly to detect changes in the sensitivity of the instrument.

For solar measurements with the diffuser, it is not possible to separate changes in instrument sensitivity from changes in the reflectance of the diffuser plate in an a priori fashion. All that can be derived from these measurements is the product of the change in the instrument and the change in the diffuser. However, there is an assumption that can tie diffuser and lunar measurements together. Basically, the change in the reflectance of the diffuser is assumed to be essentially linear over periods of one month, or so. Over longer periods, e.g., periods of one to several years, the change may turn out to be exponential, with gradually decreasing changes over time. However, this exponential change can be treated as a series of many linear segments. Experience with diffusers on previous satellite instruments has led to the assumption that diffuser degradation has been caused by the coating of the diffuser with solarized organic materials that have outgassed from the spacecraft. This accumulation process does not cause sharp step changes in the diffuser's reflectance.

Using nearly simultaneous lunar and solar diffuser measurements, it is possible to separate changes in the sensitivity of the instrument (from the lunar measurements) from changes in the reflectance of the diffuser. The time series of diffuser values will be normalized by lunar measurements. It is then possible to use the assumption of a linear change in diffuser reflectivity to identify step changes in instrument sensitivity between lunar measurements. Step changes were found in measurements with the Coastal Zone Color Scanner (CZCS), SeaWiFS' predecessor.

The initialization phase of on-orbit calibration operations, approximately the first two months after the instrument is turned on, has been designed to provide a statistically significant endpoint for the time series of SeaWiFS

calibration measurements. This is primarily the endpoint for the time series of changes in the radiometric sensitivity of the sensor. The drafting of this schedule at a point approximately six months before the launch of the instrument reduces the schedule to a "strawman," since on-orbit factors—primarily the rate of change of the reflectance of the diffuser cover—may force a modification of the schedule of events.

The following sequence provides a schedule of the calibration initialization phase of instrument operations.

1. With the solar diffuser cover on:

- Take a solar diffuser measurement at the first, safe opportunity.
- Take an interchannel measurement immediately thereafter. (This can be done at any point on orbit.)
- If possible, take a TDI measurement at the next available safe opportunity on the orbit following the diffuser measurement. Operationally, the TDI check will be about equal to a second solar diffuser measurement (see the section on TDI checks, below).
- Repeat this sequence for every downlink (twice per day) for one week. This gives 14 sets of measurements as a baseline for instrument operation. This also gives a data set to check for large changes in the reflectance of the solar diffuser cover. (Large-scale changes in the diffuser measurements will show degradation of the diffuser surface. Large-scale changes in instrument sensitivity during initial operation on orbit will be shown in measurements of the oceans.)

2. At the first full moon:

- Take a lunar measurement at a lunar phase angle of about  $7^\circ$ , going into the full moon.
- If lunar phase angles and instrument power permit, take a second lunar measurement at the same lunar phase angle coming out of the full moon. (Power restrictions may limit the measurements to one per full moon, without regard to the opportunity for a second measurement.)
- Repeat this sequence monthly for a minimum of 3–4 months. From these data, a minimum practical interval (in months) for lunar measurements for the remainder of the mission can be determined.

3. When the solar diffuser cover is removed:

- Take a solar diffuser measurement, using the diffuser cover, on one orbit.
- Take a solar diffuser measurement on the next orbit. Remove the diffuser cover during the middle of this measurement.

- Using the flight diffuser, take a solar diffuser measurement on the next orbit, followed by an inter-channel gain check and a TDI check.
  - Make a lunar measurement at the next available opportunity. It is anticipated that the solar diffuser cover will be removed one day before a lunar measurement.
  - Take a solar diffuser measurement once per downlink (twice per day) for one week to monitor any changes in the freshly exposed flight diffuser.
4. For routine operations:
- With the sequence of one every downlink, take solar diffuser measurements, TDI checks, and inter-channel gain checks. This sequence can be changed to once per week, if the stability of the instrument permits.
  - Take lunar measurements monthly. This can be changed to every other month or quarterly, if the stability of the instrument permits.

## 2.2 Solar Diffuser Calibration

Solar diffusers, such as the one designed for SeaWiFS, have been used several times on previous remote sensing satellite instruments. The series of diffuser measurements with the Solar Backscatter Ultraviolet (SBUV) spectrometer on the NIMBUS-7 satellite, and with the SBUV/2 spectrometers on the National Oceanic and Atmospheric Administration's NOAA-9 and NOAA-11 satellites, a history of the development of this technique is provided. Changes in the reflectance of the diffuser on the NIMBUS-7 SBUV were calculated using an on-orbit experiment, based on changes of the exposure rate of the diffuser for extended periods on orbit. This experiment gave an empirical model that separated changes in the SBUV spectrometer from changes in the instrument's diffuser (Cebula et al. 1988). After several years of apparently successful observations by the SBUV, it became apparent that most of the long-term changes in stratospheric ozone indicated by the instrument were not geophysical, but were instead a calibration drift within the instrument (World Meteorological Organization, 1990). The drift was determined to result from the empirical model for the diffuser reflectance. It was also found that alternate models for diffuser plate degradation could be applied to the results of the on-orbit experiment (Herman et al. 1990), with different models giving different long-term changes in stratospheric ozone.

The SBUV/2 instruments on NOAA-9 and NOAA-11 were equipped with a lamp that could be viewed either directly by the spectrometer or indirectly using the surface of the diffuser assembly (Frederick et al. 1986). By taking a series of alternating measurements of these two sources, it is possible to obtain a ratio that gives the reflectance of the diffuser. Problems with the design of the lamp on NOAA-9 prohibited the collection of long-term reflectance

measurements of its diffuser. However, corrections to the design of the NOAA-11 SBUV/2 have allowed long-term measurements of these diffuser changes. A similar, but more complicated scheme for monitoring diffuser changes has been proposed for the Moderate Resolution Imaging Spectrometer (MODIS) instrument on the Earth Observing Satellite (EOS) AM platform.

The SeaWiFS diffuser plate will be affixed to the SeaStar platform such that it faces opposite to the usual velocity vector. Sunlight will reflect off the plate for about 80 seconds as the platform pitches 5° while passing over the South Pole. For the duration of the calibration, the instrument assembly will be tilted 20° aft and the sensor will scan the diffuser plate for about 10–20 pixels along the back-scan (Fig. 1).

The solar diffuser response can be characterized by the bidirectional reflectance distribution function (BRDF) of the diffuser assembly. This function ranges above and below the nominal overall reflectance of the diffuser and is used to describe the angular dependent reflective response of the diffuser plate to incident light. The SeaWiFS diffuser BRDF can be translated to a three-dimensional table representing the spacecraft pitch, spacecraft yaw, and the instrument scan angle. It is assumed that the solar flux at the input of the diffuser assembly remains constant. The BRDF of the diffuser assembly will probably change with time as contaminants condense on the reflecting surface. To account for this change, lunar measurements are required.

The SeaWiFS instrument has eight bands with each band having four detectors. Each of the 32 detectors has its own photodiode, current-to-voltage converter, gain selection, and analog-to-digital converter. For each detector, there will be an electronic calibration pulse at the output of the current-to-voltage converter. The pulse will be recorded for about 100 pixels as part of the data stream following the diffuser plate portion of the scan. The electronic calibration pulse will have an amplitude near the maximum number of counts (1,024 counts for the 10-bit SeaWiFS data). The pulse provides a measure of inter-channel gains and eliminates the need for scanning Earth targets for gain measurements. The calibration voltage for the pulse will be summed with the output from the detector's current-to-voltage converter. Since the pulse is applied while the instrument is viewing the black, inner surface of the instrument housing, the output from the detector should be zero. However, small changes in the detector output can be removed by referencing the output from the calibration pulse to "zero" values from the readings that immediately precede and follow the pulse.

It is possible to control combinations of the detectors used in each SeaWiFS band, i.e., from a single detector, to pairs of detectors, to a combination of all four. For test purposes on orbit, each detector for individual bands can be viewed independently. Table 1 gives the five possible TDI configurations. During the initial gain checks,

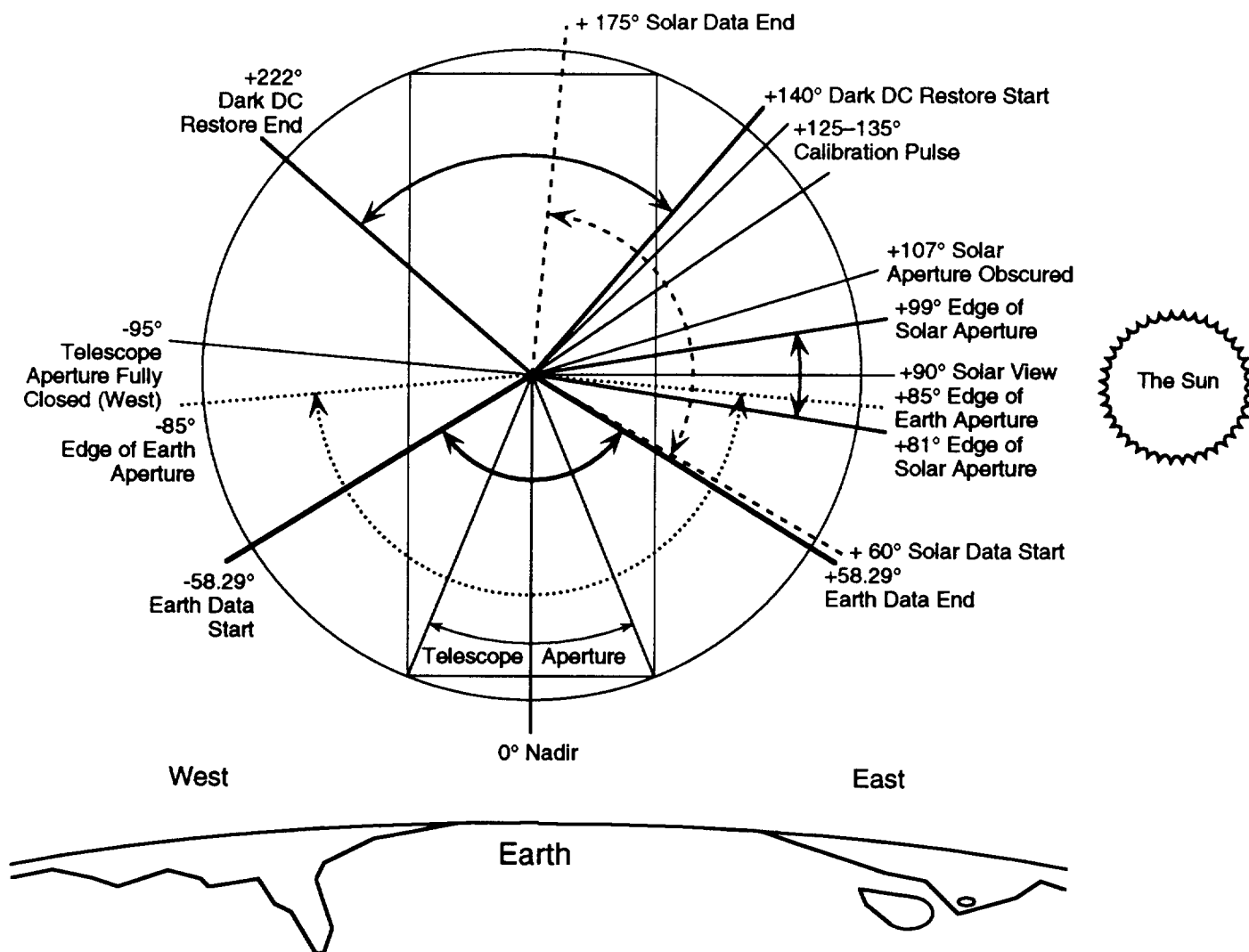


Fig. 1. Scanning angles of SeaWiFS instrument for solar calibrations.

the stability of the calibration voltage can be checked by cycling through the gain sequence ( $g_i$ ) shown in Table 2. The set of  $g_1$  values before and after each other gain gives a check of the constancy of the calibration voltage over the measurement period. For this type of check of relative values, a constant input value (or a well-characterized, slowly changing value) is necessary. Knowledge of the absolute value of the input is not required.

Table 1. TDI configurations with the corresponding detector arrangements.

Configuration	Detector Arrangement
1	Det1 + Det2 + Det3 + Det4
2	Det1 summed with itself 4 times
3	Det2 summed with itself 4 times
4	Det3 summed with itself 4 times
5	Det4 summed with itself 4 times

Table 2. Gain sequences for TDI configurations. Start and stop times are in seconds.

Configuration	Gain Sequence	Start	Stop
1	$g_1, g_2, g_1, g_3, g_1, g_4, g_1$	0	7
2	$g_1, g_2, g_1, g_3, g_1, g_4, g_1$	7	14
3	$g_1, g_2, g_1, g_3, g_1, g_4, g_1$	14	21
4	$g_1, g_2, g_1, g_3, g_1, g_4, g_1$	21	28
5	$g_1, g_2, g_1, g_3, g_1, g_4, g_1$	28	35
1	$g_1, g_2, g_1, g_3, g_1, g_4, g_1$	35	42
2	$g_1, g_2, g_1, g_3, g_1, g_4, g_1$	42	49
3	$g_1, g_2, g_1, g_3, g_1, g_4, g_1$	49	56
4	$g_1, g_2, g_1, g_3, g_1, g_4, g_1$	56	63
5	$g_1, g_2, g_1, g_3, g_1, g_4, g_1$	63	70
1	$g_1, g_2, g_1, g_3, g_1, g_4, g_1$	70	77

The scan in the solar calibration mode will produce a data stream identical in form to a typical SeaWiFS (high resolution) Local Area Coverage (LAC) scan. Fig. 2 shows

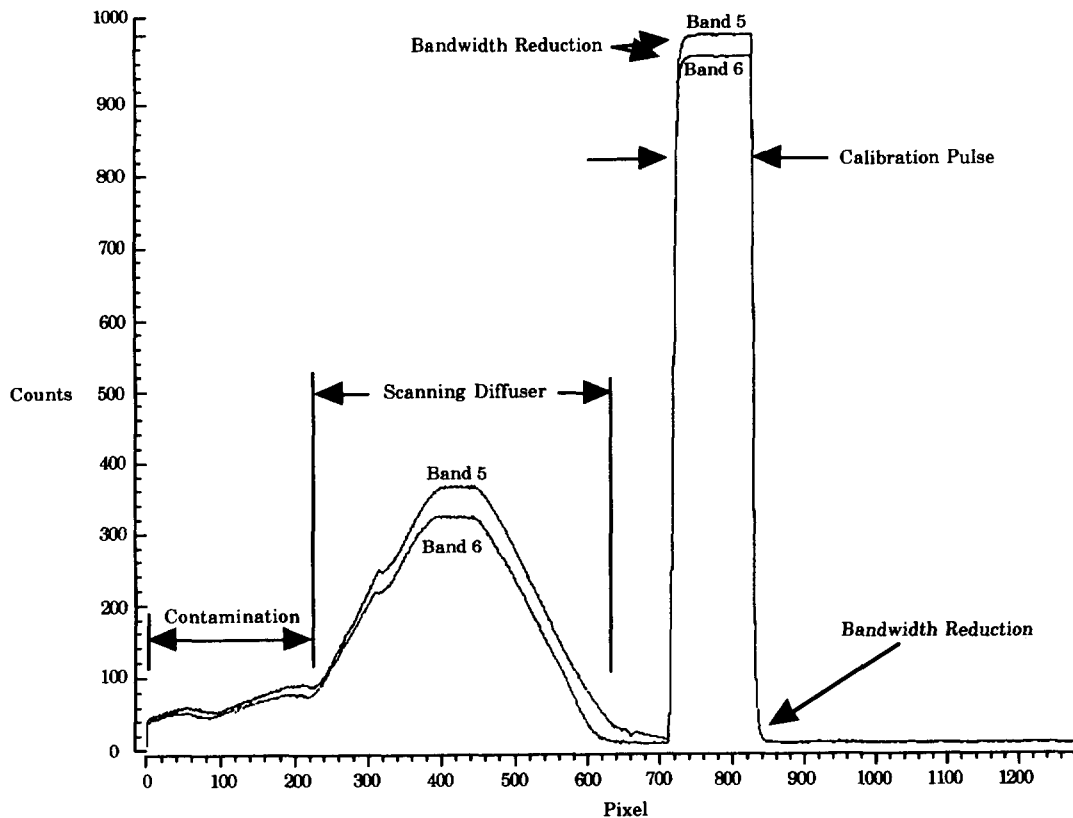


Fig. 2. Response of SeaWiFS channels 5 and 6 during an experimental solar calibration.

the response of two of the SeaWiFS channels for an experimental solar calibration. The diffuser is viewed in the sensor response for about 400 pixels from start to finish, and the calibration pulse follows about 100 pixels downstream. The anomalously high readings in the first few hundred pixels (before scanning the diffuser) are a result of possible solar reflectance contamination from the small gap between the diffuser and the telescope housings. The portion of the scan that views the diffuser exhibits a nearly linear ramping to and from a maximum plateau. The ramp occurs as the instrument scans from deep space, onto the diffuser and then onto the black, inner-surface of the back of the instrument. As can also be seen in Fig. 2, the calibration pulse produces a curved signal as it transitions to the maximum value around pixel number 700 and again as it transitions to the background value around pixel 840. This curved response is a result of a bandwidth reduction which is applied to reduce high frequency noise in the signal.

### 2.2.1 Diffuser Calibration Model

The solar calibration model is designed to simulate the LAC data stream of a solar calibration for various test scenarios. Solar irradiances from Neckel and Labs (1984) for selected channels are read into the model from a database on CALVAL. The irradiance data are integrated to the Sea-

WiFS bands using a full-width at half-maximum (FWHM) approximation. The model simulates a diffuser scan by considering the intersection area of two circles which are in relative movement. The circles represent the instantaneous field-of-view (IFOV) of the sensor and of the aperture covering the solar diffuser plate. In the algorithm, the circles are aligned such that the  $y$  locations of the circle centers are identical, and the initial  $x$  locations of the circle centers are set by the user. The IFOV circle is then moved in a stepwise fashion in the  $x$  direction relative to the aperture circle and the intersection area is computed for each step. The intersection area  $A_i$  is defined as follows (see also Fig. 3):

$$A_i = \frac{r_1^2(\theta_1 - \sin \theta_1)}{2} + \frac{r_2^2(\theta_2 - \sin \theta_2)}{2}, \quad (2)$$

where  $r_1$  is the radius of circle one,  $r_2$  is radius of circle two,  $\theta_1$  is the intersection angle of circle one, and  $\theta_2$  is intersection angle of circle two.

The normalized intersection area is obtained by dividing  $A_i$  by the area of the smaller circle, which defines the maximum intersection area. The normalized areas of intersection for each step are translated to ramping coefficients, i.e., the ratio of the sampled value to the actual value, which are then applied as multiplicative factors to each pixel in succession along the scan. This intersection

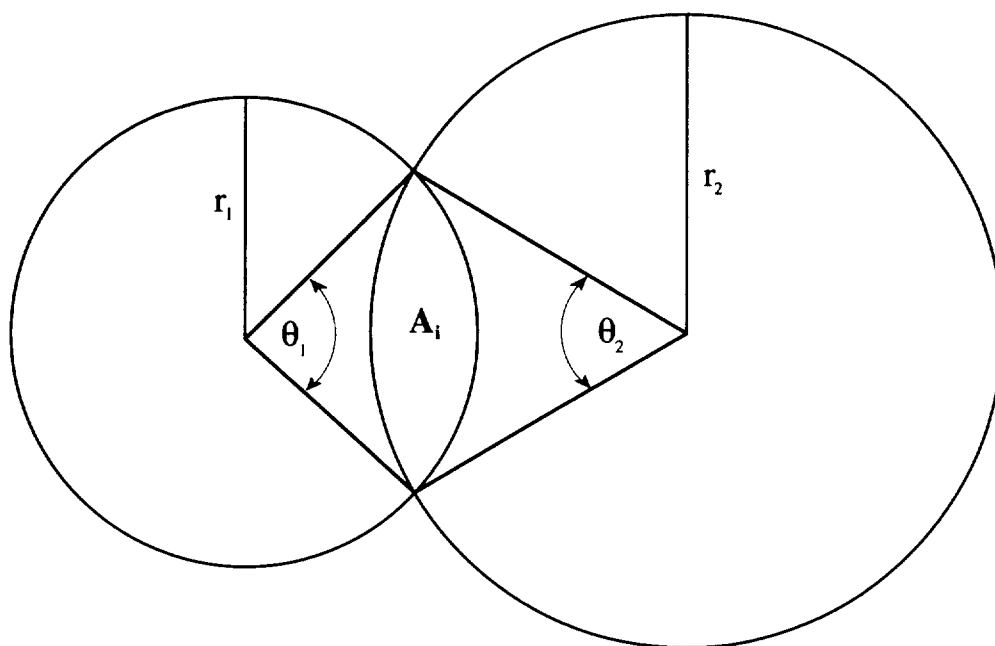


Fig. 3. The area of intersecting circles,  $A_i$ .

GUI Parameters		
25	10	ENTER FACTOR : 0.3
X CENTER OF IFOV	ALBEDO OF DIFFUSER	ENTER FACTOR : 0.85
400	1	ENTER FACTOR : 0.95
X CENTER OF APERTURE	SOLAR ZENITH ON DIFFUSER	ENTER FACTOR : 0.98
75	10	ENTER FACTOR : 1.0
RADIUS OF IFOV	SOLAR AZIMUTH ON DIFFUSER	ENTER FACTOR : 1.0
100	MAGNITUDE OF CALIBRATION PULSE (%)	ENTER FACTOR : 1.0
RADIUS OF APERTURE	700	ENTER FACTOR : 1.0
1	START OF CALIBRATION PULSE	ENTER FACTOR : 1.0
INCREMENT OF IFOV	850	ENTER FACTOR : 1.0
1	END OF CALIBRATION PULSE	ENTER FACTOR : 1.0
CHANNEL		DONE
TITLE: <input type="text"/>		

Fig. 4. The initial GUI for the solar calibration model.

algorithm produces a symmetric pattern for a scan with quasi-linear ramp-up and ramp-down intervals bracketing a period of fixed maximum output. A simulated calibration pulse may also be inserted in the modeled signal following the above diffuser pattern. The simulated pulse produces a stepwise jump in the signal and, therefore, does not accurately model the curved response produced by bandwidth reduction in the transition to maximum and again to background (see Fig. 2).

Fig. 4 shows the solar calibration model GUI. These input values may be adjusted to simulate various calibration scenarios for selected SeaWiFS channels (CHANNEL). For instance, the lengths and amplitudes of both the sensor response to the diffuser and the calibration pulse can be adjusted by modifying the input values on the GUI. The center of the intersecting circles (X CENTER OF IFOV and X CENTER OF APERTURE), the sizes of the circles (RADIUS OF IFOV and RADIUS OF APERTURE), and the scan movement (INCREMENT OF IFOV) determine the lengths of the ramp-up, maximum, and ramp-down intervals for the simulated diffuser measurement. ENTER FACTOR modifies the ramping coefficients by applying multiplicative factors to the coefficients determined by the above circle intersection algorithm. In addition, the value entered in ALBEDO OF DIFFUSER is applied as a multiplicative factor and can therefore be used to simulate diffuser degradation.

ZENITH ON DIFFUSER and AZIMUTH ON DIFFUSER refer to the angle of the incident sunlight on the diffuser and are used for retrieving BRDF values from a three-dimensional lookup table. The third dimension in this table is linked to the scan angle of the sensor. This value is a function only of pixel number and is computed automatically in the algorithm. The calibration pulse can be modeled using MAGNITUDE OF CALIBRATION PULSE % which sets the maximum value for a pulse by applying a percentage of the Neckel and Labs (1984) irradiance for the given channel. START OF CALIBRATION PULSE and END OF CALIBRATION PULSE assigns start and end pixel numbers for the pulse within the scan.

### 2.2.2 Diffuser Calibration Model Results

Figs. 5–7 show three representations of the modeled instrument response of a solar calibration for the criteria listed in Fig. 4 and a flat BRDF field, i.e., all BRDF values set to unity. In this example, X CENTER OF IFOV, X CENTER OF APERTURE, and INCREMENT OF IFOV are chosen in such a manner as to produce about a 375 pixel start-to-finish response of the diffuser induced signal. The simulated calibration pulse is modeled to be 150 pixels wide with a maximum amplitude equal to the saturation radiance value. The total calibration is simulated to span 82.4 seconds which corresponds to 494 SeaWiFS scans. Additional ramping to phase in and out of the lunar sweep is also modeled using intersecting circles producing a total of 592 scans. Fig. 5 shows a nearly linear ramping to max-

imum and back for the diffuser portion of a single scan agreeing in general with the laboratory results shown in Fig. 2. Also included in this figure is the simulated calibration pulse.

In Fig. 6, a two-dimensional representation of the calibration is shown with the  $x$  coordinate representing the instrument scan and the  $y$  coordinate representing time. A three-dimensional representation of the same output is provided in Fig. 7. Fig. 8 shows the same calibration, except with a random BRDF field applied as a three-dimensional lookup table. The three dimensions on the diffuser represent the incident solar zenith angle, the incident solar azimuth angle, and the pixel number (viewing angle of the sensor). The prelaunch BRDF measurements from the Hughes/Santa Barbara Research Center (SBRC) will be substituted as input to the solar model when testing is completed. The addition of this information to the model will prove useful in tracking post-launch diffuser and sensor performance.

## 2.3 Lunar Calibration

Observations of the diffuser assembly will not be used to monitor long-term changes in the instrument's radiometric sensitivity. Rather, for this purpose, the instrument will make a series of measurements of the surface of the moon during the lifetime of the SeaWiFS mission. It is assumed that the lunar surface has stabilized over geologic time and that the reflectance of the surface will not change over the 5-year mission of SeaWiFS. It is also assumed that the solar irradiance will be known from sources outside of the SeaWiFS measurement. Solar diffuser measurements will be used to fill in the gaps between lunar measurements, which cannot be made more often than once per month. The diffuser measurements will be normalized to the lunar values at the measurement times.

To maintain consistency, lunar calibrations can occur only about once a month when the lunar phase angle is within  $7^\circ$  of full phase. When this criterion is satisfied on selected orbits, the SeaStar platform will undergo a  $360^\circ$  tilt maneuver on the back-orbit allowing the sensor to produce a standard LAC data stream of the lunar surface. Given a nominal SeaStar pitch rate of about  $0.15^\circ \text{ s}^{-1}$ , it is expected that the moon will encompass about 7 SeaWiFS pixels at the lunar equator and about 20 SeaWiFS scan lines from lunar pole-to-lunar pole.

### 2.3.1 Lunar Calibration Model Description

The lunar calibration model simulates the sensor response of a SeaWiFS lunar viewing for varying instrument and spacecraft conditions. Table 3 provides a synopsis of the user interfaces for the model. The means and standard deviations for both the integrated scanned moon and the scanned central nine pixels are written to a specified output file which is used for subsequent statistical analysis. An output display is also produced, consisting of the

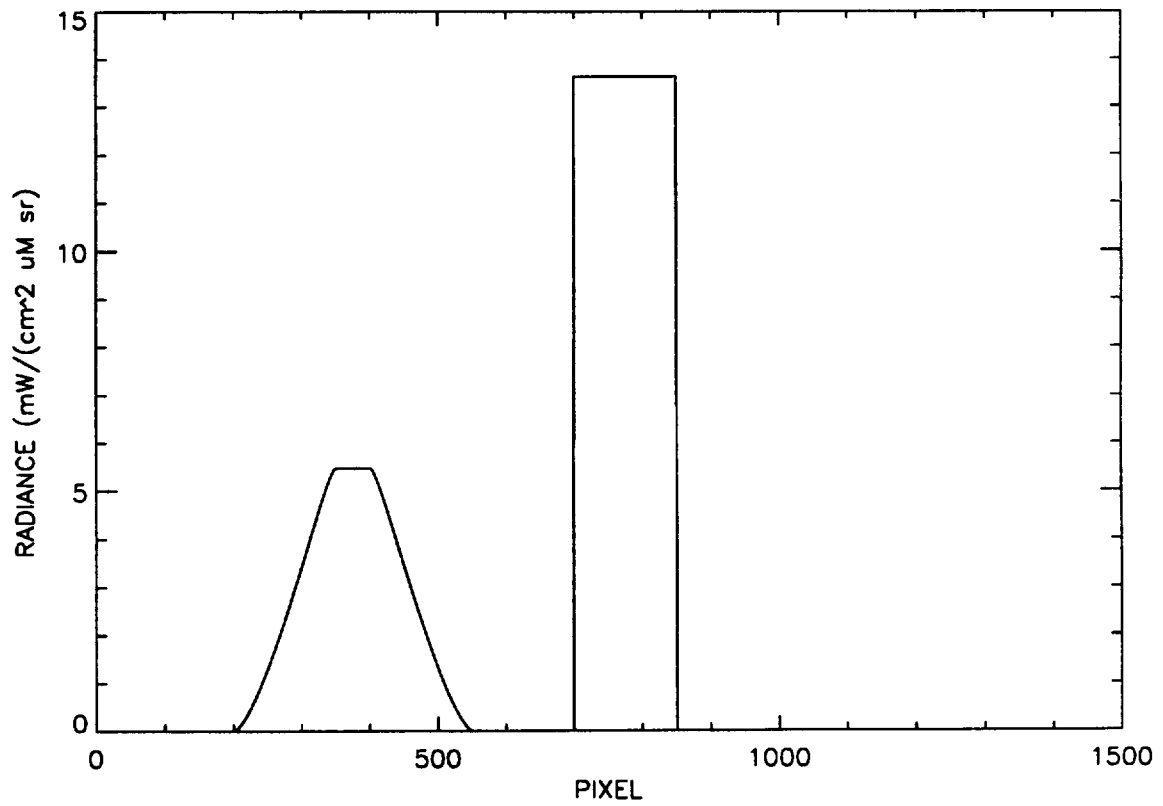


**Fig. 5.** A single scan of the solar diffuser measurement (including a calibration pulse) produced by the solar calibration model.

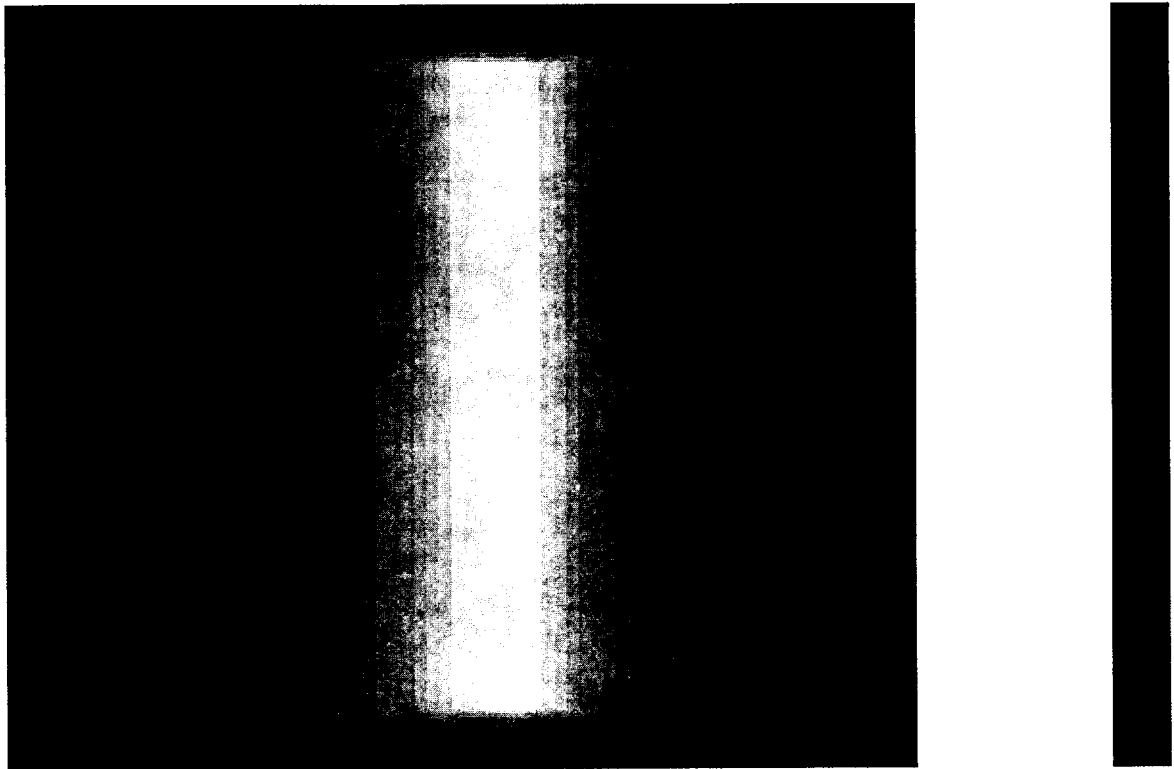


**Fig. 6.** A two-dimensional representation of the solar diffuser measurement (including a calibration pulse) produced by the solar calibration model.

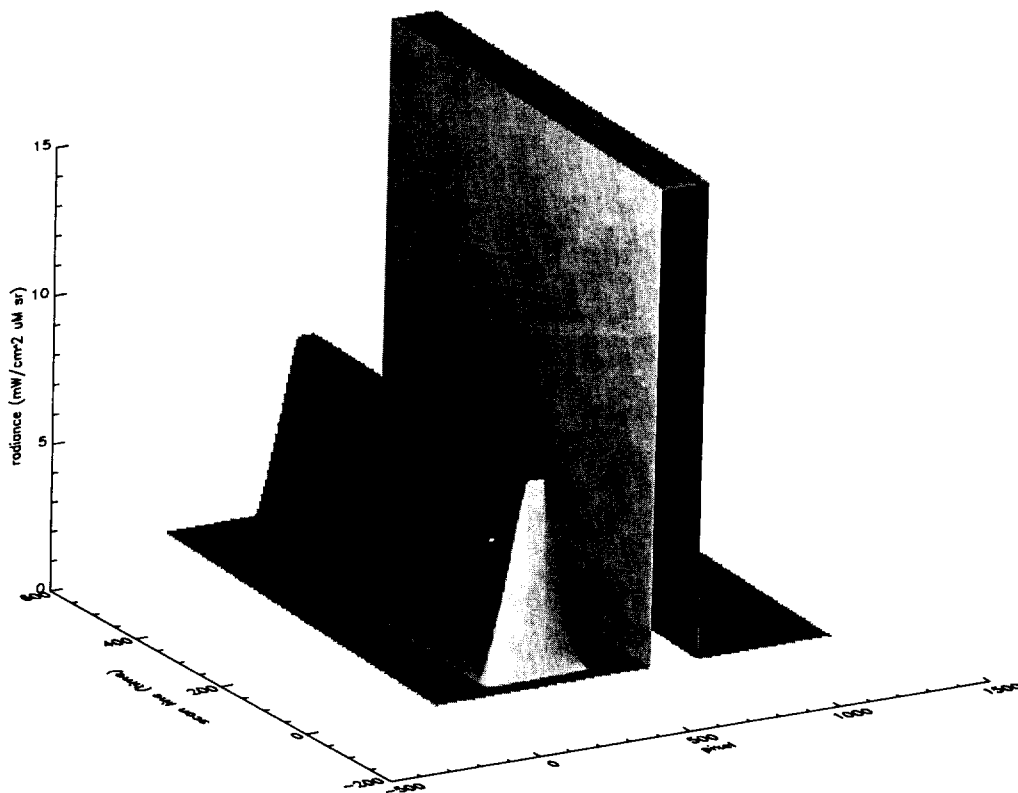


**Fig. 7.** A three-dimensional representation of the solar diffuser measurement (including a calibration pulse) produced by the solar calibration model.

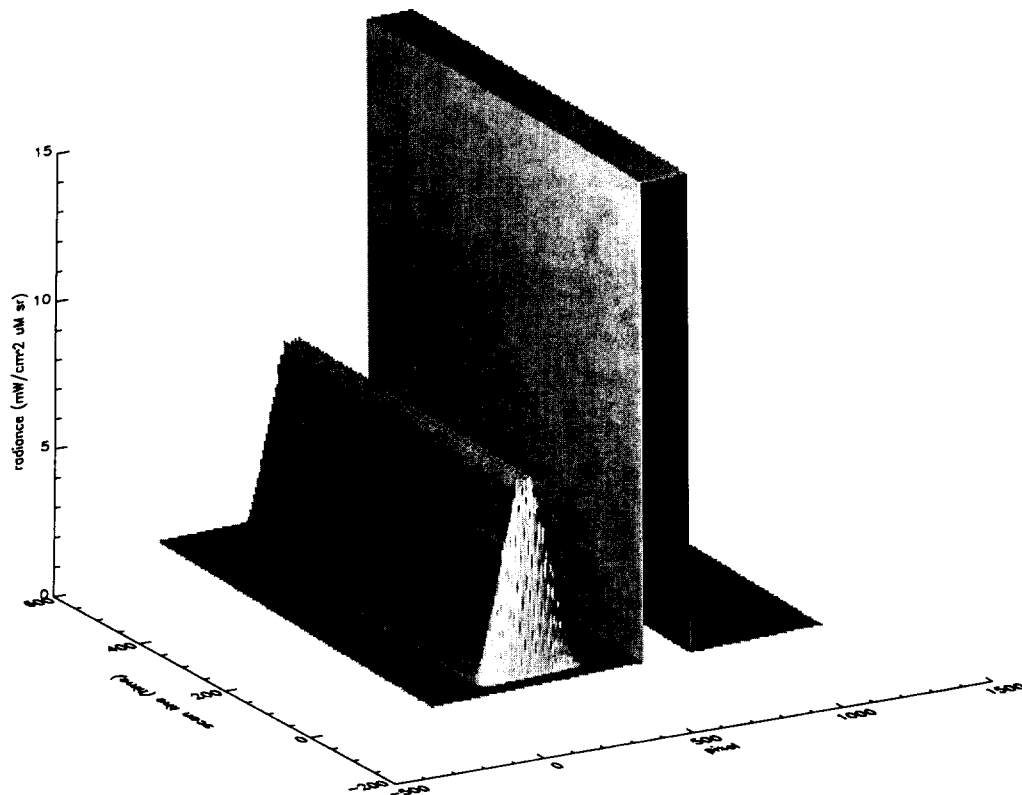


**Fig. 8.** The same as Fig. 7 except with a random BRDF field read as input for the solar calibration model.

original lunar image and the output following each model step listed in Table 3 (scanned image, scanned image with bright-to-dark response, and scanned image with bright-to-dark and dark-to-bright response).

**Table 3.** User interfaces for the lunar calibration model.

Interface	Function	Inputs
SCANMOON	Simulates the image of the moon recorded for a lunar calibration.	<ul style="list-style-type: none"> <li>Image size,</li> <li>Scan resolution,</li> <li>Scan position,</li> <li>Channel,</li> <li>Sensor degradation,</li> <li>Gain, and</li> <li>Output filename.</li> </ul>
DRK2BRT	Simulates the dark-to-bright response of the sensor.	<ul style="list-style-type: none"> <li>Ringing and</li> <li>Ramp-up factors.</li> </ul>
BRT2DRK	Simulates the bright-to-dark response of the sensor.	<ul style="list-style-type: none"> <li>Ringing and</li> <li>Ramp-down factors.</li> </ul>

Fig. 9 shows the initial GUI of the lunar calibration model. The size of the input image is specified with **X IMAGE SIZE** and **Y IMAGE SIZE**, respectively. The scan pixel size and scan line sampling are adjustable by setting **SCANSIZE** and **SCANSTEP**, respectively. Initial pixel and line position are determined by **START X SCAN** and **START Y SCAN**. The simulated SeaWiFS pixels are constructed by computing the mean of all input image pixels within a square of size **SCANSIZE**  $\times$  **SCANSIZE**. The corner of each square is determined by pointers incremented in the  $x$  direction by **SCANSIZE** and in the  $y$  direction by **SCANSTEP**. This separation of  $x$  and  $y$  pointer movement allows oversampling or subsampling in the  $y$  direction, thus permitting the modeling of platform rotation rates.

Variance in pixel registration can be tested using **START X SCAN** and **START Y SCAN** to initialize the pointer to a pixel and line on the input image. Loss of instrument sensitivity can be simulated using **SENSOR DEGRADATION**, which applies the specified percent decrease in range to the input image. Selecting **CHANNEL** initiates a query to the CALVAL database to obtain the wavelength dependent solar irradiance from Neckel and Labs (1984). A gain factor can be input to the model by entering a value in the **ENTER GAIN** prompt.

The user interfaces shown in Figs. 10 and 11 provide inputs to routines for simulating the dark-to-bright and bright-to-dark target responses of the instrument. The ramp-up and ramp-down factors are specified by the **ENTER FACTOR** prompts. A ringing response is triggered when the absolute value of the difference in successive values exceeds **THRESHOLD**. This ringing will last for **N PERIOD** pixels and

has a damped periodic function specified in **ENTER PERIOD** and **AMPLITUDE**. For example, the following events occur if the values shown in Fig. 10 are chosen:

1. If the difference in successive pixels exceeds the value of **THRESHOLD**, ramping occurs over the subsequent five pixels. These pixels are factored by 0.3, 0.85, 0.95, 0.98, and 1.00 (**ENTER FACTOR**), respectively, simulating the response to a bright target. If **THRESHOLD** is not exceeded, then the five pixels are factored by the quantity:  $\text{FACTOR}/(\Delta P/\text{THRESHOLD})$ , where  $\Delta P$  is the difference in successive pixels. If this value exceeds 1.00 it is set equal to 1.00.
2. If the difference in successive pixels exceeds the value of **THRESHOLD**, a delayed ringing response is triggered. The ringing commences when successive downstream pixels remain equal or decrease in magnitude. The ringing occurs for 6 pixels (**N PERIOD**) employing a periodic wave of  $8\pi$  rad. (**ENTER PERIOD**) with wave amplitude specified as  $1 \text{ mW cm}^{-2} \mu\text{m}^{-1} \text{ sr}^{-1}$  (**AMPLITUDE**). The wave function is characterized by a damped sine wave using a  $\sin(x)/x$  function, where  $x$  is the pixel number within the scan line.

The user can adjust the frequency, amplitude, and duration of the ringing by altering the input values for the lunar model. Fig. 12 shows the modeled ringing of a single scan for four selected scenarios. High amplitude and low amplitude ringing are shown in panels a) and b), respectively; variations in the ringing periodicity are shown in panels c) and d).

### 2.3.2 Lunar Calibration Model Results

A high resolution (16 bit) lunar image at  $3^\circ$  phase (Kieffer, pers. comm.) was read as input for the lunar calibration model. Fig. 13 shows an example of the display output obtained from the model. The upper left panel shows the original Kieffer moon, the lower left shows the scanned moon, the upper right shows the scanned moon with the dark-to-bright response applied, and the lower right shows the scanned moon with both the dark-to-bright and the bright-to-dark responses applied. In this example, the model input values were adjusted such that the scanned moon was 7 pixels wide and 22 scan lines high. The total integrated mean of the moon and the mean of the central nine pixels are also displayed for each model step.

A test was performed using the lunar calibration model to determine the effects on the calibration of variable pixel registration of the lunar surface. A total of 15 runs were produced in which  $x$  pixel positions (along scan lines) were moved at one-fourth SeaWiFS pixel increments while holding the  $y$  pixel position (scan lines) constant; and  $y$  pixel positions were then moved at one-twelfth pixel increments while holding the  $x$  pixel position constant. For this series of runs, an extreme case of ringing was applied. The initial

The GUI window is titled "SCANMOON". It contains the following elements:

- X IMAGE SIZE:** A slider with a value of 851.
- Y IMAGE SIZE:** A slider with a value of 851.
- SCANSIZE:** A slider with a value of 85.
- SCANSTEP:** A slider with a value of 30.
- START X SCAN:** A slider with a value of 0.
- START Y SCAN:** A slider with a value of 0.
- SENSOR DEGRADATION:** A slider with a value of 0.
- ENTER GAIN :** A text input field containing "2.0".
- ENTER TITLE :** An empty text input field.
- ENTER OUTPUT FILE :** A text input field containing "stats".
- CHANNEL:** A vertical slider on the right side of the window.
- DONE:** A button at the bottom right of the window.

Fig. 9. Initial GUI for the lunar calibration model.

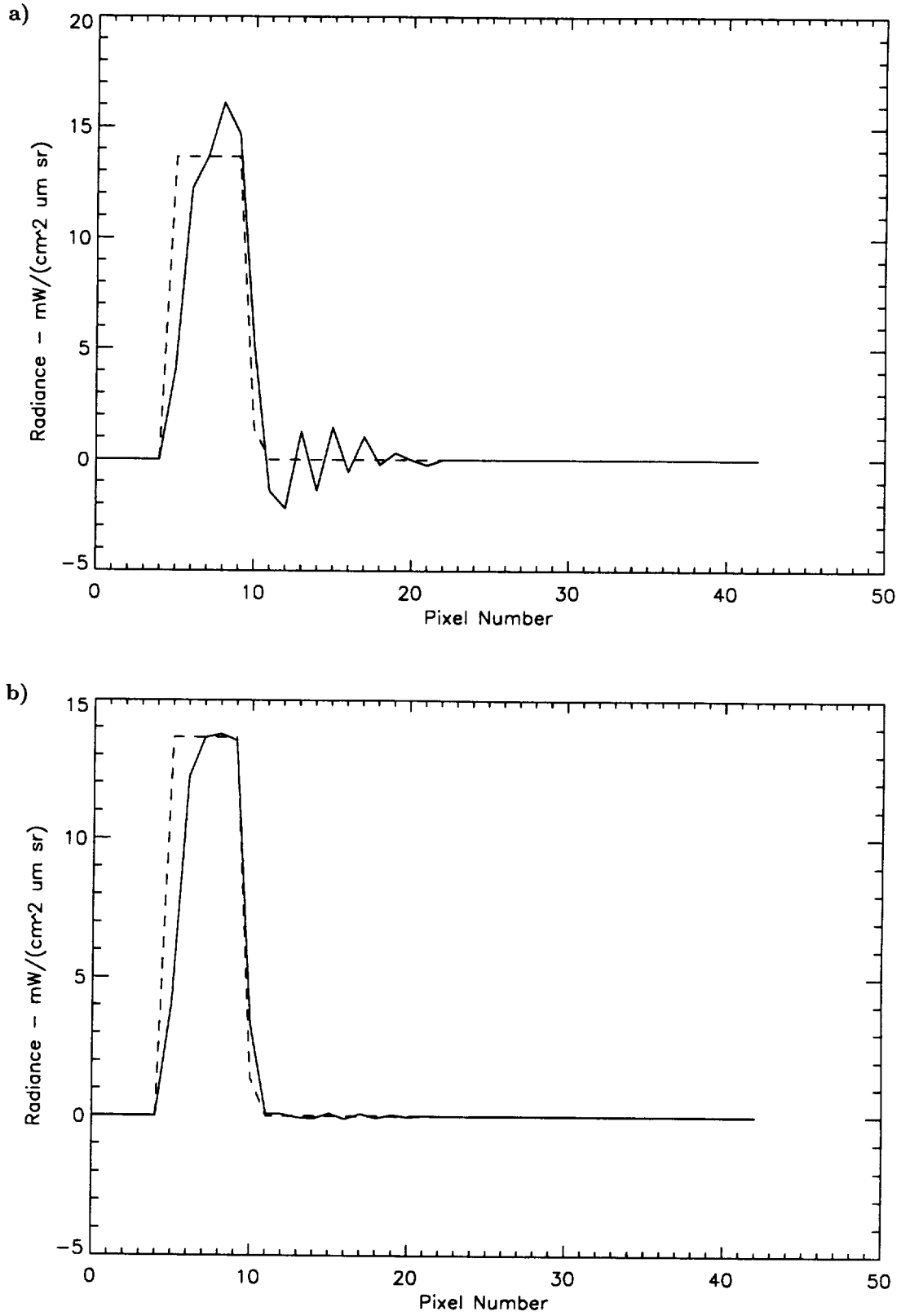
The GUI window is titled "DRK2BRT". It features three sliders on the left side, each with a numerical label above it: "THRESHOLD" (range 0 to 2, current value 2), "N PERIOD" (range 0 to 6, current value 6), and "AMPLITUDE" (range 0 to 1, current value 1). Below the "THRESHOLD" slider is an input field labeled "ENTER PERIOD :" with the value "1440". To the right of the sliders is a vertical column of eight input fields, each labeled "ENTER FACTOR :". The values in these fields are: 0.3, 0.85, 0.95, 0.98, 1.0, 0.0, 0.0, and 0.0. At the bottom of this column is a button labeled "DONE".

Fig. 10. GUI for the dark-to-bright instrument response in the solar calibration model.

The image shows a graphical user interface (GUI) window titled "BRT2DRK". The window is divided into several sections. On the left, there are three main input areas: "THRESHOLD" with a slider set to -2, "N PERIOD" with a slider set to 6, and "AMPLITUDE" with a slider set to 1. Below the "THRESHOLD" and "N PERIOD" sliders, there is a text input field labeled "ENTER PERIOD :" containing the value "1440". On the right side of the window, there is a vertical stack of eight "ENTER FACTOR :" input fields, each containing a numerical value: 0.7, 0.15, 0.05, 0.02, 0.0, 0.0, 0.0, and 0.0. At the bottom of this stack is a "DONE" button.

Section	Parameter	Value
THRESHOLD	Slider	-2
	ENTER PERIOD :	1440
N PERIOD	Slider	6
	ENTER PERIOD :	1440
AMPLITUDE	Slider	1
	ENTER PERIOD :	1440
FACTORS	ENTER FACTOR :	0.7
	ENTER FACTOR :	0.15
	ENTER FACTOR :	0.05
	ENTER FACTOR :	0.02
	ENTER FACTOR :	0.0
	ENTER FACTOR :	0.0
	ENTER FACTOR :	0.0
	ENTER FACTOR :	0.0
DONE		

Fig. 11. GUI for the bright-to-dark instrument response in the solar calibration model.



**Fig. 12.** Ringing from the lunar calibration model for a) high amplitude ringing, b) low amplitude ringing. Note: the dashed line is the target and the solid line is the response.

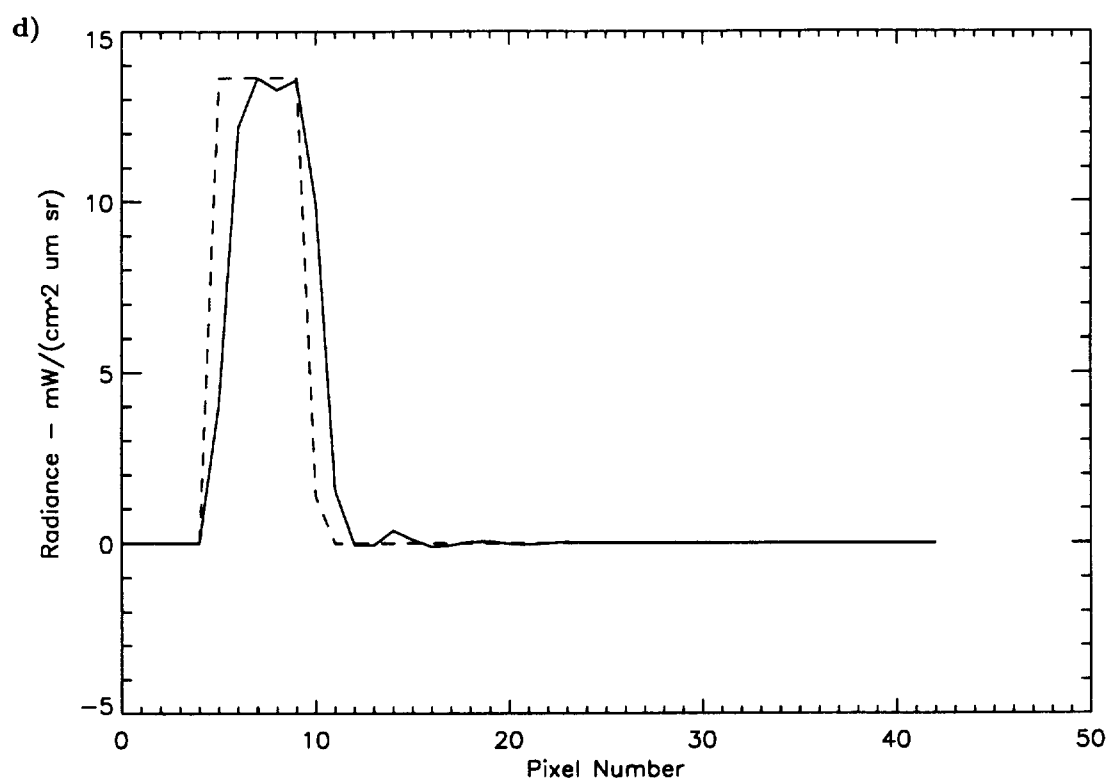
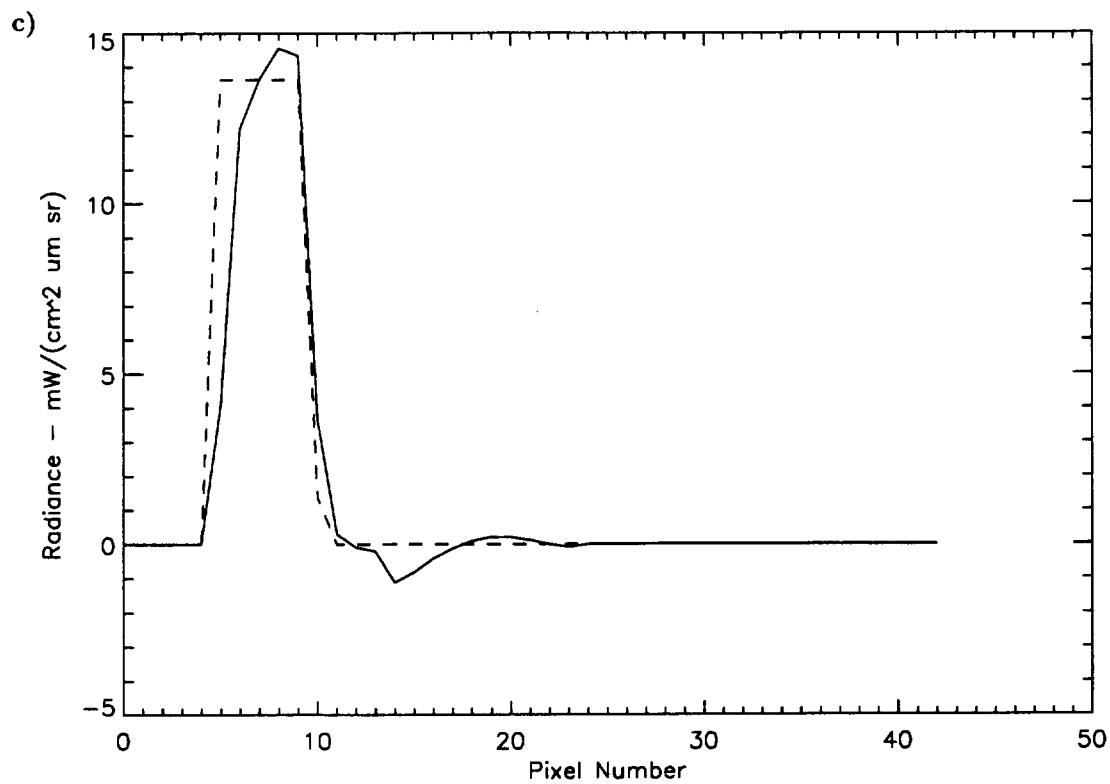


**Fig. 12. (cont.)** Ringing from the lunar calibration model for c) high frequency ringing, and d) low frequency ringing.

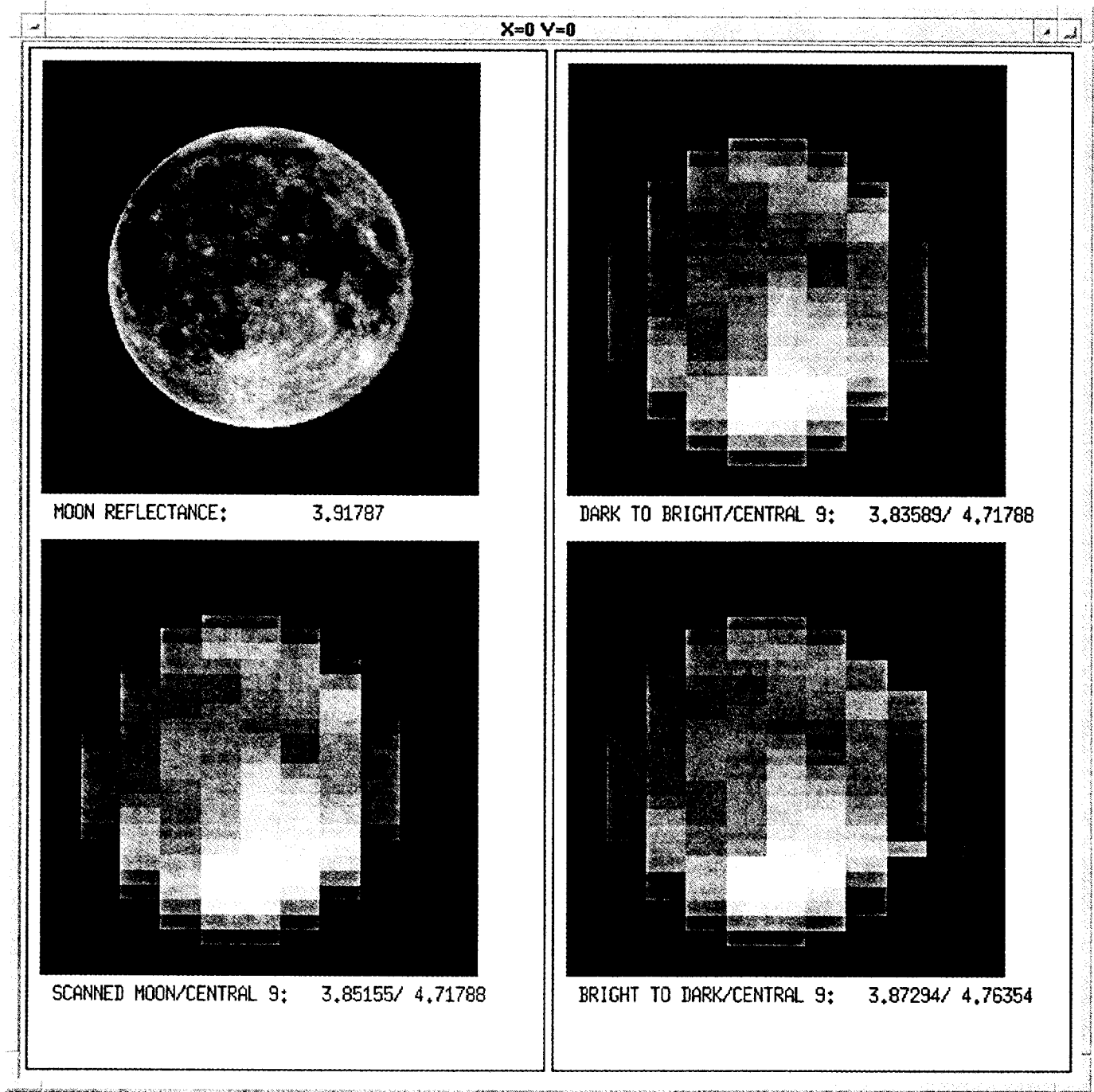
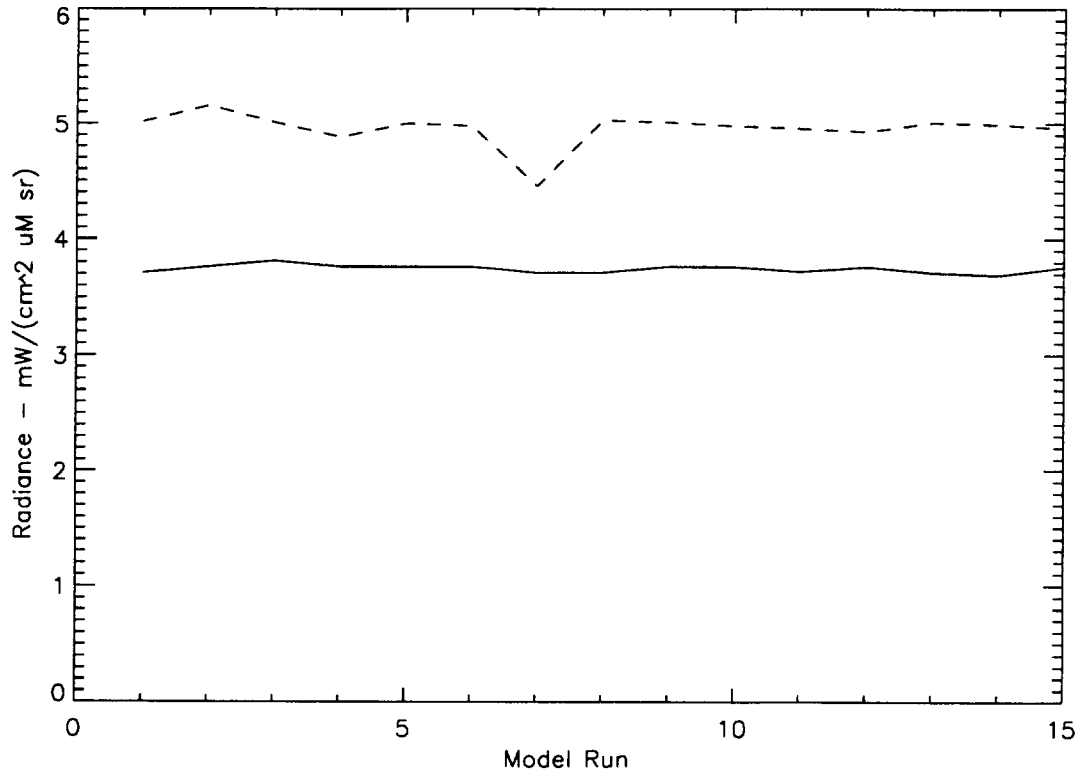
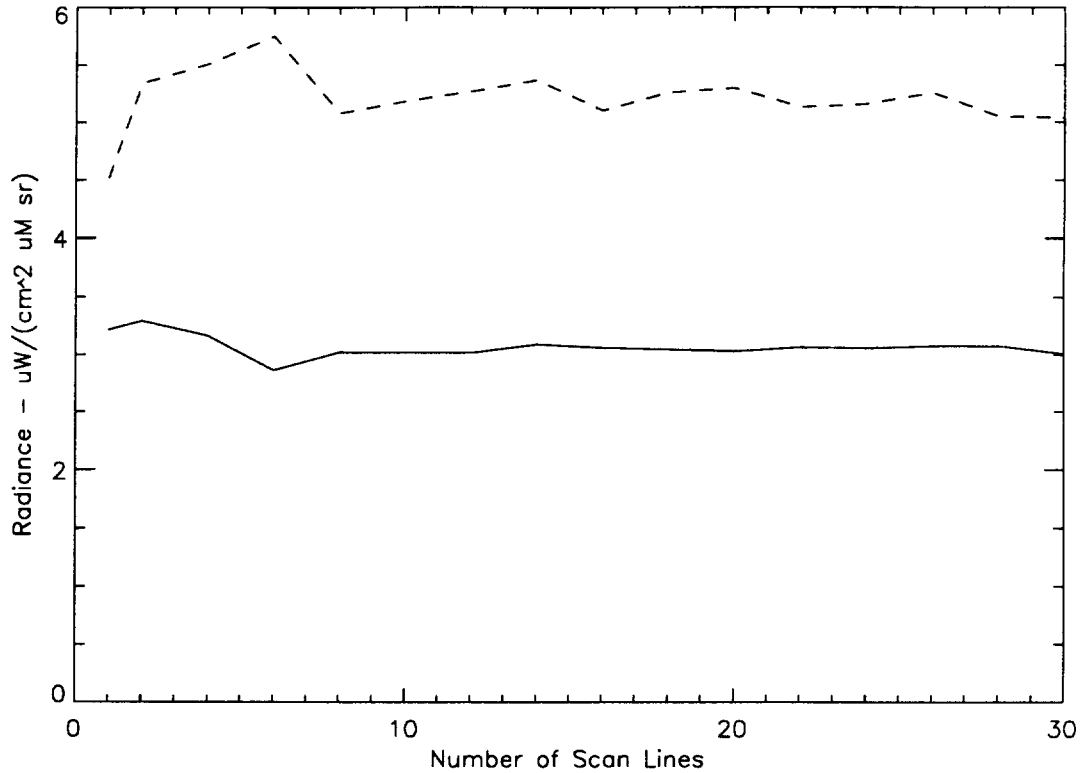


Fig. 13. Display output from the lunar calibration model.



**Fig. 14.** Stability of the lunar measurements as a function of pixel registration for the integrated lunar mean (solid line) and the central 9-pixel mean (dashed line).



**Fig. 15.** Stability of the lunar measurements as a function of the number of scan lines for the integrated lunar mean (solid line) and the central 9-pixel mean (dashed line).

amplitude of the ringing was set to  $1 \text{ mW cm}^{-2} \mu\text{m}^{-1} \text{ sr}^{-1}$ , and the ringing period was set to  $8\pi$  rad. The results were tabulated for each step of the model for both the integrated image mean and the central 9-pixel ( $3 \times 3$ ) mean (Table 4). Standard deviations ( $\sigma$ ) of the model output over the runs were computed for each model step as a measure of stability. Fig. 14 shows the retrieved mean radiances for both the mean integrated image and the mean central 9 pixels as a function of pixel registration. These results indicate the retrieved radiances from the lunar calibration are more stable, as indicated by the standard deviations, for the integrated mean than the central 9-pixel mean. The relative instability of the central 9-pixel mean among calibrations is most likely a result of variable lunar reflectance as the  $3 \times 3$  sampling box changes position with regard to the lunar surface.

Another test, using the lunar calibration model, was conducted to determine the effects of varying the number of scan lines across the moon. This test illustrates the impact of variable platform rotation rates upon lunar calibrations. The results are tabulated in Table 5 and displayed in Fig. 15. The integrated mean is again found to be more stable than the central 9-pixel mean in tracking lunar reflectance.

These modeling studies can be compared to a ground-based sweep of the moon by the SeaWiFS instrument at Goleta, California on December 9, 1992. On this date, the moon was sampled shortly after a lunar eclipse giving a very small lunar phase angle. Fig. 16 shows the Kieffer moon, the modeled lunar scan, and four observed sweeps of the moon. The observed lunar scans were not corrected for atmospheric interference, which possibly accounts for the discrepancies between the observations and the modeled scan. The scan at 1922 Pacific Standard Time (PST) was scanned from the top to the bottom producing an upside-down view in comparison to the other images in the figure.

An important consideration for the solar and lunar observation data is the potential for ghost images in the optical path of the instrument. These artifacts occur around bright targets and are a result of reflections off of the polarization scrambler, which is the third component in the SeaWiFS optical path (Fig. 17). The light reflected off the polarization scrambler exhibits two artificial images on either side of pixels in the direction perpendicular to the scan (Holmes, pers. comm.) as shown in Fig. 18. These artifacts contain about 3% of the signal and are confined to about 4 pixels of the target edge. In Fig. 16, the observed lunar scans exhibit little or no evidence of ghost images. Fig. 19 shows a three-dimensional representation of the lunar sweep from opposite perspectives at 1922 PST for channel 6. In this figure, the natural logarithm of SeaWiFS counts has been plotted as the vertical coordinate. There appears to be some elevated values in the direction perpendicular to the scan from pixels 9–15.

Side-to-side differences in the half-angle mirror (Fig. 17) will be characterized at SBRC before launch. There may

be changes in the side-to-side characteristics of the half-angle mirror during the course of the mission. The change in the average for the two mirror sides cannot be determined independently on orbit and must be part of the long-term sensitivity of the instrument. The average is an inherent part in the 20 scans that cover the surface of the moon and in the 480 scan lines of a diffuser measurement. The magnitude of the side-to-side differences in the half-angle mirror, however, can be tracked during standard measurements of the instrument's diffuser. During each diffuser measurement, there are 240 side1-side2 pairs of half-angle differences to be used for calculations. These differences transform into scan line-to-scan line differences in the ocean measurements. The magnitude of the scan-to-scan differences will be tracked in the onboard calibration information although, strictly speaking, these differences are not part of the radiometric calibration for the instrument.

### 2.3.3 Additional Considerations

Several factors are likely to impact the measured lunar reflectance with the SeaWiFS instrument. One of these factors is the eccentricity of the lunar orbit. The lunar orbit places the moon 356,410 km from the Earth at perigee, and 406,697 km at apogee. Over the course of a lunar orbit, the Earth-moon distance ( $\xi_{EM}$ ) can be expressed as (Duffett-Smith 1979):

$$\xi_{EM} = \frac{a(1 - e^2)}{1 + e \cos[M'_m + 6.289 \sin(M'_m)]} \quad (3)$$

where  $a$  is the semi major axis,  $e$  is the eccentricity, and  $M'_m$  is the corrected mean anomaly, which is a function of date, and refers to an imaginary moon in a circular orbit.

Assuming an inverse square distance relationship for the observed lunar reflectance, the amount of lunar radiance measured by SeaWiFS can vary by as much as 30% over all possible full moon orbital positions. Observed lunar radiance may also be dependent, to a lesser extent, on the moon-sun distance. Lunar observations will therefore require normalization to account for the variable Earth-moon and sun-moon distances. In addition to the variable radiance, pixel registration will vary as a result of the change in distance between the sensor and the moon. This latter consideration may be allayed by using the integrated lunar surface for the SeaWiFS observations, as discussed in Section 2.3.2. Additional functionality will be added to the lunar calibration model to simulate the potential effects of an elliptical orbit.

Libration is another possible source of uncertainty for the SeaWiFS lunar observations. The major motions of the Earth-moon system allow observers on Earth, over a period of time, to view 59% of the lunar surface, even though the same side of the moon is always facing the Earth. Longitudinal libration occurs because the moon

**Table 4.** Lunar observation model results for testing calibration stability as a function of variable pixel registration. All units are in  $\text{mW cm}^{-2} \mu\text{m}^{-1} \text{sr}^{-1}$ . As a measure of stability, standard deviations ( $\sigma$ ) of the model output over the runs are reported.

$x$ Pixel Offset	$y$ Pixel Offset	<i>Integrated</i>			<i>Central Nine</i>		
		Scan	Dark-Bright	Bright-Dark	Scan	Dark-Bright	Bright-Dark
0	0	3.71	2.83	2.33	5.02	5.19	4.17
1/4	0	3.76	2.86	2.31	5.16	5.25	3.80
2/4	0	3.81	2.86	2.30	5.01	4.45	5.26
3/4	0	3.76	2.74	2.26	4.88	5.21	4.71
0	1/12	3.76	2.89	2.37	5.00	5.24	4.14
0	2/12	3.76	2.87	2.24	4.98	4.96	4.23
0	3/12	3.71	2.84	2.32	4.45	4.89	4.15
0	4/12	3.71	2.81	2.32	5.03	5.22	4.18
0	5/12	3.76	2.88	2.37	5.01	5.15	4.15
0	6/12	3.76	2.87	2.36	4.98	4.99	4.24
0	7/12	3.72	2.84	2.33	4.96	4.97	4.17
0	8/12	3.76	2.86	2.32	4.93	4.84	4.18
0	9/12	3.71	2.83	2.33	5.01	5.17	4.16
0	10/12	3.69	2.90	2.36	4.99	5.00	4.25
0	11/12	3.76	2.89	2.36	4.96	4.92	2.21
Column $\sigma$		0.03	0.04	0.04	0.06	0.14	0.33

**Table 5.** Lunar observation model results for testing calibration stability as a function of a variable number of scan lines. All units are in  $\text{mW cm}^{-2} \mu\text{m}^{-1} \text{sr}^{-1}$ . As a measure of stability, standard deviations ( $\sigma$ ) of the model output over the runs are reported.

Number of Scan Lines	<i>Integrated</i>			<i>Central Nine</i>		
	Scan	Dark-Bright	Bright-Dark	Scan	Dark-Bright	Bright-Dark
1	3.60	3.12	3.22	4.36	4.52	4.52
2	4.24	3.47	3.29	4.96	5.34	5.34
4	4.18	3.21	3.16	5.31	5.42	5.51
6	3.60	2.93	2.86	5.43	5.71	5.75
8	3.81	3.05	3.02	4.90	5.05	5.08
10	3.64	3.05	3.02	4.96	4.96	5.18
12	3.64	3.04	3.02	4.10	5.26	5.27
14	3.82	3.14	3.09	4.91	5.35	5.37
16	3.73	3.08	3.06	4.98	5.08	5.10
18	3.71	3.12	3.05	5.01	5.22	5.26
20	3.70	3.10	3.03	5.02	5.26	5.30
22	3.75	3.13	3.06	4.96	5.08	5.13
24	3.72	3.12	3.06	4.98	5.12	5.16
26	3.72	3.12	3.08	5.01	5.22	5.30
28	3.77	3.14	3.08	4.98	5.03	5.05
30	3.70	3.05	3.01	4.97	5.01	5.04
Column $\sigma$	0.18	0.11	0.10	0.22	0.26	0.26

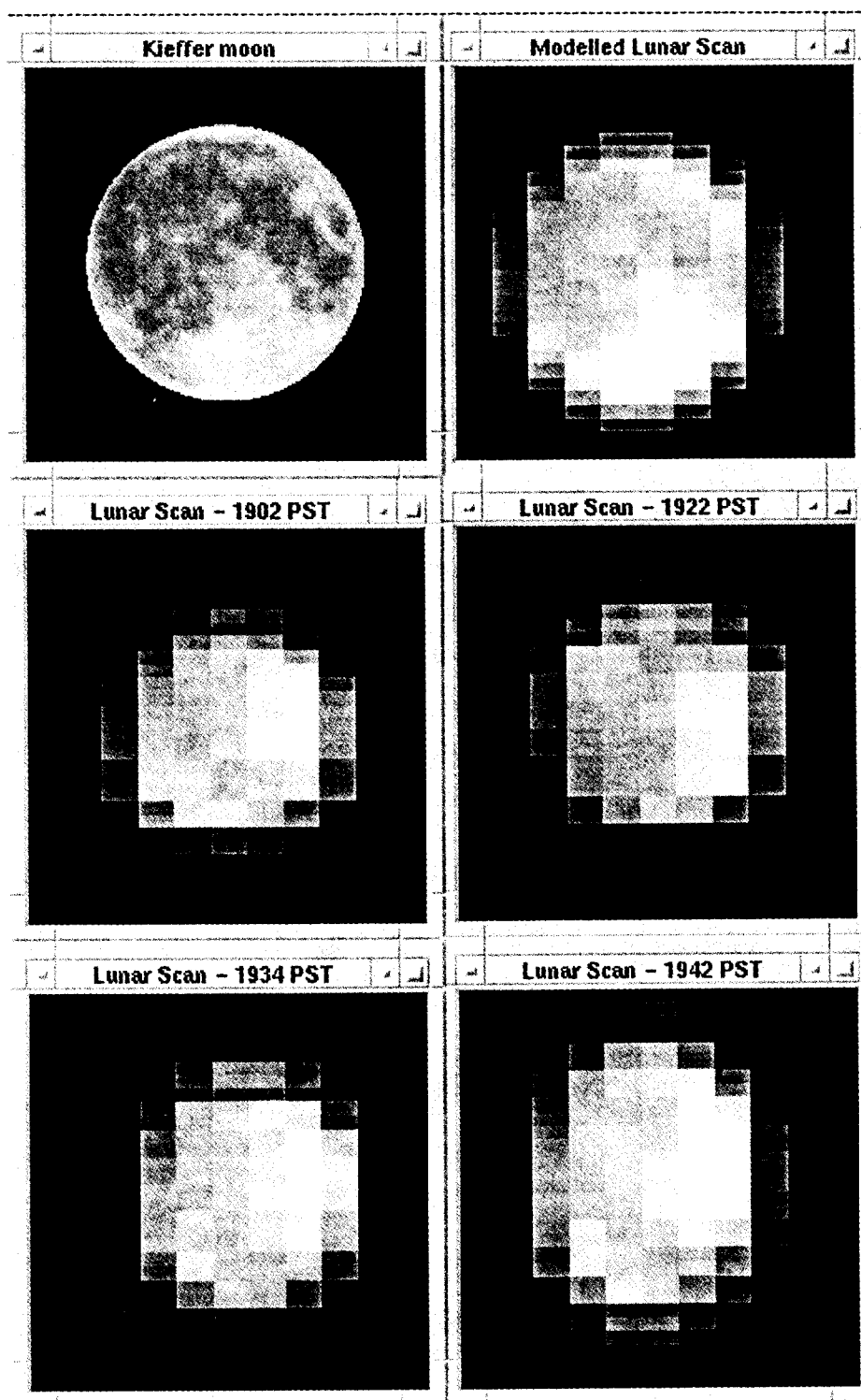


Fig. 16. Comparison of modeled lunar scan to ground-based measurements.

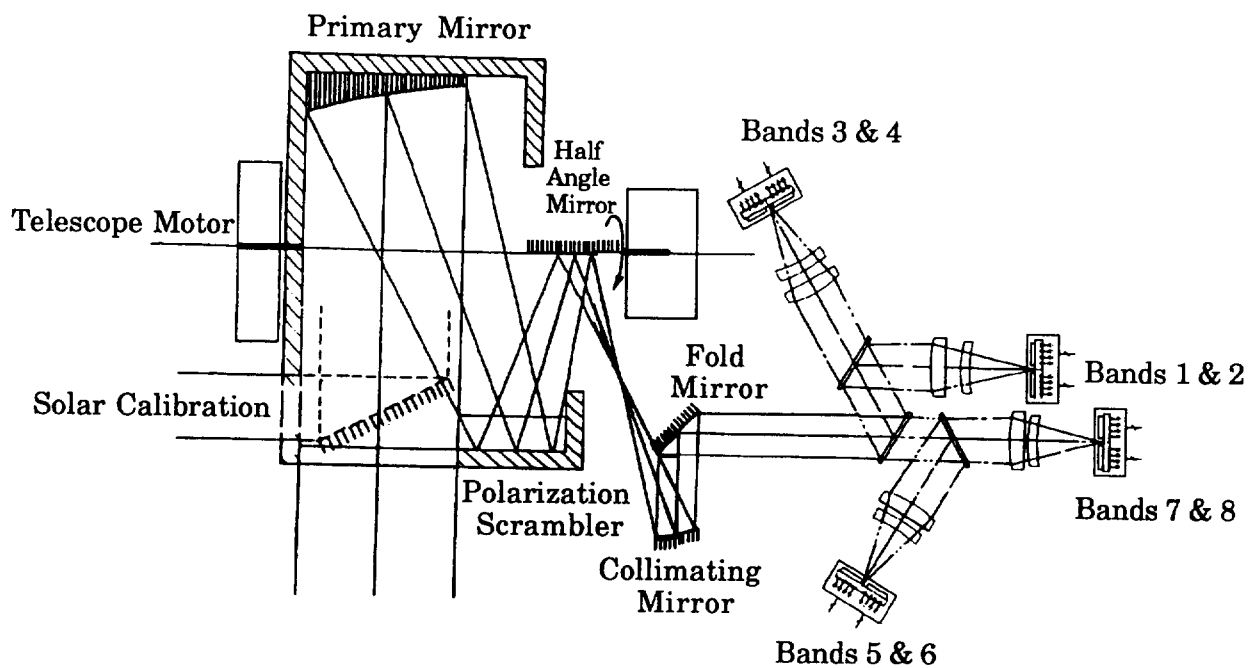


Fig. 17. A schematic of the SeaWiFS optical layout.

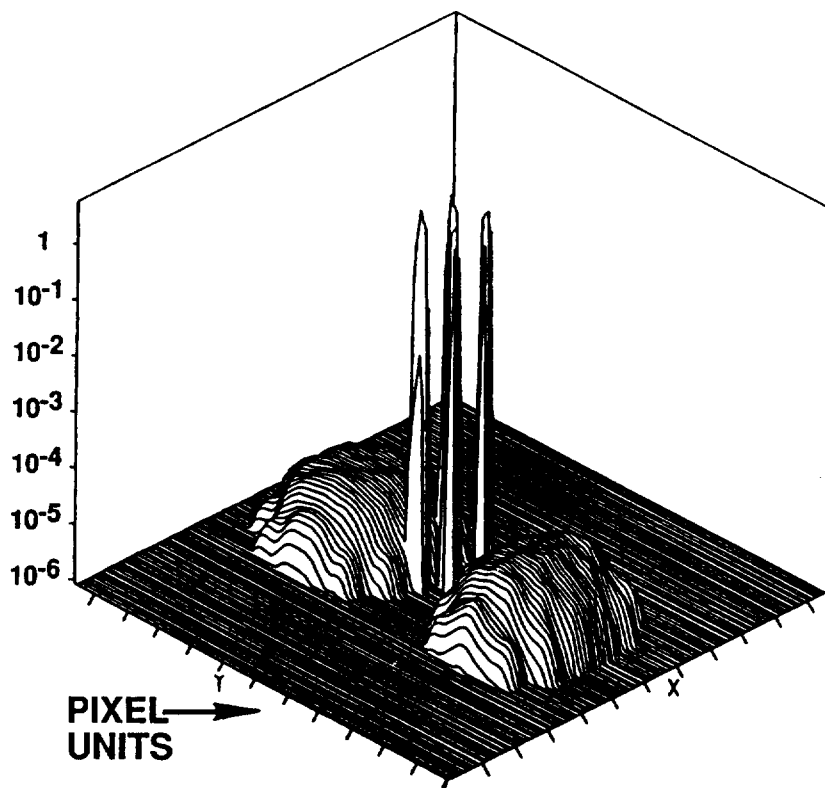


Fig. 18. Ghost images induced by the polarization scrambler.

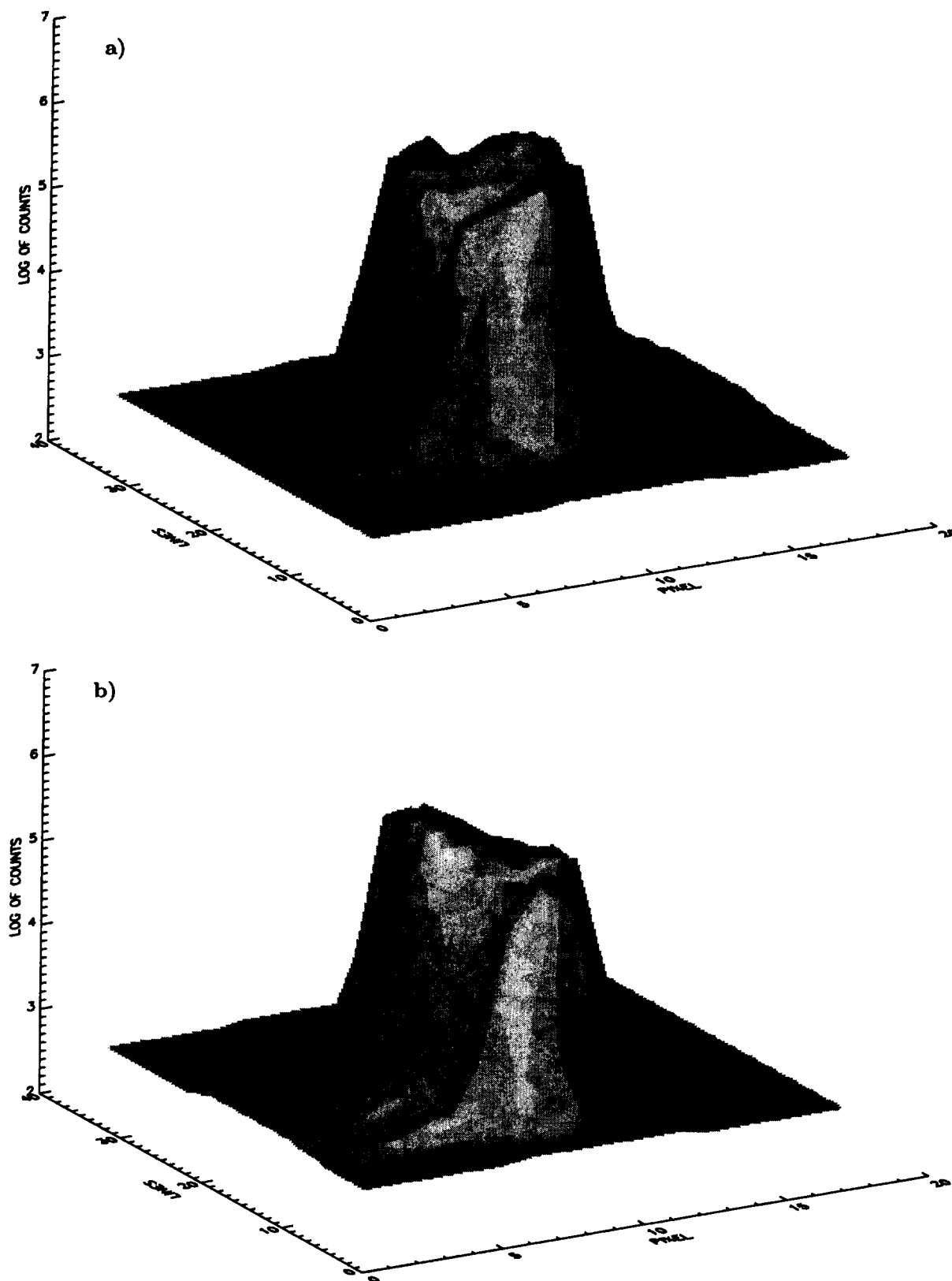


Fig. 19. A three-dimensional representation of a) the lunar sweep at 1922 PST for channel 6 and b) the same scene from the opposite perspective (180° difference).

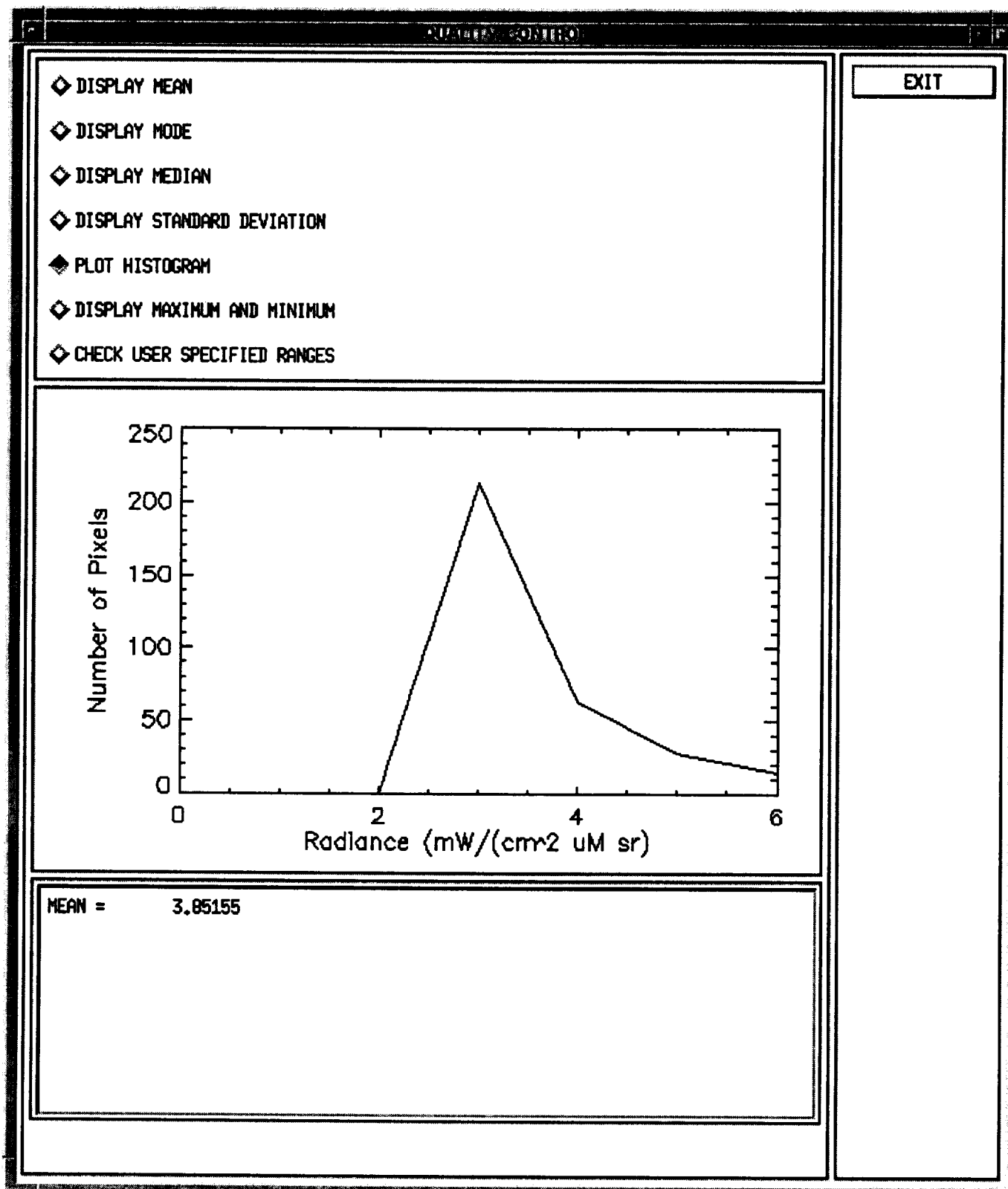


Fig. 20. GUI for the calibration data and instrument telemetry quality control routines.

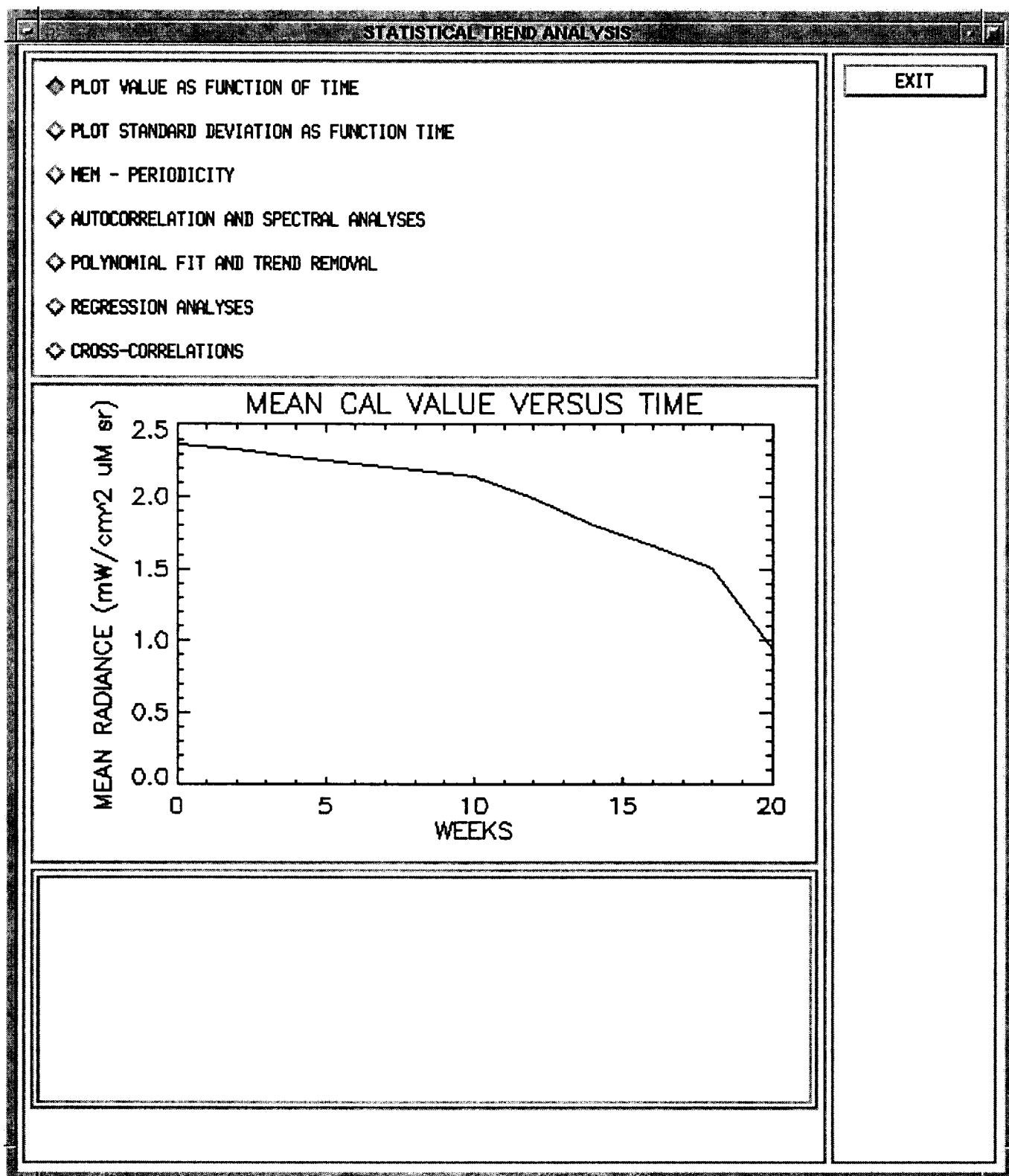


Fig. 21. GUI for the calibration data and instrument telemetry trend analysis routines.

rotates on its axis at a constant rate but travels around the Earth at varying velocities due to the elliptical orbit. Latitudinal libration is a result of the  $6.7^\circ$  tilt in the lunar axis with regards to the Earth ecliptic. The obvious effect of libration is that the sensor will not always be viewing the same complete face of the moon. To correct for this effect, a database of lunar observations can be populated with respect to libration.

### 3.0 QUALITY CONTROL

Quality control routines will be essential for ensuring the integrity of the calibration data. It is anticipated that most of this activity will be activated in an automated fashion. However, user intervention routines can be implemented using interfaces such as the prototype presented in Fig. 20. Statistics are generated by using this interface to check for outliers or unusual patterns in the data. The user can select from three types of data average: mean, mode, and median. The standard deviation can be generated to check for unexpected variance in the data. Outliers can be determined by selecting for the minimum and maximum value.

The user can also choose to specify a valid range of data. Unusual or unexpected patterns in the data can be checked by selecting the histogram option. The example in Fig. 20 shows a histogram applied to radiances from a simulated lunar calibration.

### 4.0 TREND ANALYSIS

Trends in both the calibration and instrument telemetry data will require analysis, since patterns in these data may display drift or periodicity. An accurate resolution of these effects will allow corrective techniques to be applied to the data. For example, polynomial or periodic functions may be implemented to compensate for any observed trends.

Fig. 21 shows a prototype interface for trend analysis. The selections activate routines that are designed to both characterize and compensate for trends in the instrument calibration and telemetry data. In the example from this figure, a simulated degradation in the lunar calibration has been plotted as a function of day. Since a calibration reading may be composed of the mean of several pixels, the user can also track the trend of calibration scatter by plotting the standard deviation as a function of time.

Periodicity in the data can be analyzed by selecting the **AUTOCORRELATION AND SPECTRAL ANALYSIS** and **MEM - PERIODICITY** options. The maximum entropy method (MEM) is used to deduce periodicity when data are not evenly spaced in time. Regressions and cross-correlations can be generated to check for relationships among calibration or telemetry parameters. Finally, trends in the data can be removed through the use of polynomial fitting algorithms.

## 5.0 RECOMMENDATIONS

Modeling results from the lunar calibration indicate the integrated mean of the entire lunar surface is a more stable measure than the mean of a central grouping of pixels. This conclusion was reached by considering possible uncertainties in the pixel registration and platform rotation rates. In addition, there may be some evidence of optical artifacts, i.e., ghost images, in the SeaWiFS signals. The magnitude of these artifacts is small in comparison to the lunar signals, but the impact on calibrations remains uncertain. More analysis of ghost images may be required.

Another consideration is to use the prelaunch sensor characterizations, when available from the SBRC, to modify the solar and lunar models. The models can be made to conform to the new data and to test the transfer of prelaunch data to orbit. An additional enhancement to the models will include the input of the actual BRDF table from SBRC. Following launch, the models can be used to evaluate the actual performance of the sensor-diffuser system.

### ACKNOWLEDGMENTS

The authors would like to thank Watson Gregg for use of the solar irradiance data integrated to SeaWiFS bands.

### GLOSSARY

BRDF	Bidirectional Reflectance Distribution Function
CALVAL	Calibration/Validation
CZCS	Coastal Zone Color Scanner
EOS	Earth Observing Satellite
FWHM	Full-Width at Half-Maximum
GSFC	Goddard Space Flight Center
GUI	Graphical User Interface
IDL	Interactive Data Language
IFOV	Instantaneous Field-Of-View
LAC	Local Area Coverage
MEM	Maximum Entropy Method
MODIS	Moderate Resolution Imaging Spectrometer
NASA	National Aeronautics and Space Administration
NIMBUS	Not an acronym—a series of NASA experimental weather satellites containing a wide variety of atmosphere, ice, and ocean sensors.
NIST	National Institute of Standards and Technology
NOAA	National Oceanic and Atmospheric Administration
PST	Pacific Standard Time
SBRC	(Hughes) Santa Barbara Research Center
SBUV	Solar Backscatter Ultraviolet Sensor
SeaWiFS	Sea-viewing Wide Field-of-view Sensor
SGI	Silicon Graphics, Incorporated
TDI	Time Delay Integration

# Modeling of the SeaWiFS Solar and Lunar Observations

## SYMBOLS

- $a$  Semi-major axis of the Earth's orbit.
- $A_i$  The intersection area.
- $D$  Sequential day of the year.
- $e$  Orbit eccentricity of the Earth.
- $F_0$  Solar irradiance corrected for the Earth-sun distance.
- $\overline{F}_0$  Mean solar irradiance.
- $M'_m$  The corrected mean orbit anomaly of the Earth, which is a function of date, and refers to an imaginary moon in a circular orbit.
- $r_1$  The radius of circle one.
- $r_2$  The radius of circle two.
- $x$  The pixel number within a scan line.
- $\Delta P$  The difference in successive pixels.
- $\theta_1$  The intersection angle of circle one.
- $\theta_2$  The intersection angle of circle two.
- $\xi_{EM}$  The distance between the Earth and the moon.
- $\sigma$  Standard deviation of a set of data values.

## REFERENCES

- Cebula, R.P., H. Park, and D.F. Heath, 1988: Characterization of the Nimbus-7 SBUV radiometer for the long term monitoring of stratospheric ozone, *J. Atmos. Ocean. Technol.*, **5**, 215–227.
- Duffett-Smith, P., 1979: Practical astronomy with your calculator, Cambridge University Press, New York, NY, 129 pp.
- Frederick, J.E., R.P. Cebula, and D.F. Heath, 1986: Instrument characterization for detection of long-term changes in stratospheric ozone: An analysis of the SBUV/2 radiometer, *J. Atmos. Ocean. Technol.*, **3**, 472–480.
- Gordon, H.R., D.K. Clark, J.W. Brown, O.B. Brown, R.H. Evans, and W.W. Broenkow, 1983: Phytoplankton pigment concentrations in the Middle Atlantic Bight: comparison of ship determination and CZCS estimates, *Appl. Opt.*, **22**, 20–36.
- Herman, J.R., R.D. Hudson, and G.N. Serafino, 1990: An analysis of the 8 year trend in ozone depletion from alternate models of SBUV instrument degradation, *J. Geophys. Res.*, **95**, 7,403–7,416.
- McClain, C.R., W.E. Esaias, W. Barnes, B. Guenther, D. Endres, S. Hooker, G. Mitchell, and R. Barnes, 1992: Calibration and validation plan for SeaWiFS, *NASA Tech. Memo. 104566*, Vol. 3, S.B. Hooker and E.R. Firestone, Eds., 41 pp.
- Neckel, H. and D. Labs, 1984: The solar radiation between 3300 and 12500 Å, *Solar Phys.*, **90**, 205–258.
- World Meteorological Organization, 1990: Report of the International Ozone Trends Panel, 1988: *World Meteorological Organization Global Ozone Research and Monitoring Project, Report No. 18*, 2 Vols., Geneva, Switzerland.

# REPORT DOCUMENTATION PAGE

Form Approved  
OMB No. 0704-0188

Public reporting burden for this collection of information is estimated to average 1 hour per response, including the time for reviewing instructions, searching existing data sources, gathering and maintaining the data needed, and completing and reviewing the collection of information. Send comments regarding this burden estimate or any other aspect of this collection of information, including suggestions for reducing this burden, to Washington Headquarters Services, Directorate for Information Operations and Reports, 1215 Jefferson Davis Highway, Suite 1204, Arlington, VA 22202-4302, and to the Office of Management and Budget, Paperwork Reduction Project (0704-0188), Washington, DC 20503.

<b>1. AGENCY USE ONLY (Leave blank)</b>		<b>2. REPORT DATE</b> May 1993	<b>3. REPORT TYPE AND DATES COVERED</b> Technical Memorandum	
<b>4. TITLE AND SUBTITLE</b> SeaWiFS Technical Report Series Volume 10--Modeling of the SeaWiFS Solar and Lunar Observations			<b>5. FUNDING NUMBERS</b>  970.2	
<b>6. AUTHOR(S)</b> Robert H. Woodward, Robert A. Barnes, Charles R. McClain, Wayne E. Esaias, William L. Barnes, and Ann T. Mecherikunnel Series Editors: Stanford B. Hooker and Elaine R. Firestone				
<b>7. PERFORMING ORGANIZATION NAME(S) AND ADDRESS(ES)</b> Laboratory for Hydrospheric Processes Goddard Space Flight Center Greenbelt, Maryland 20771			<b>8. PERFORMING ORGANIZATION REPORT NUMBER</b>  93B00085	
<b>9. SPONSORING/MONITORING AGENCY NAME(S) AND ADDRESS(ES)</b> National Aeronautics and Space Administration Washington, D.C. 20546-0001			<b>10. SPONSORING/MONITORING AGENCY REPORT NUMBER</b>  TM-104566, Vol. 10	
<b>11. SUPPLEMENTARY NOTES</b> Robert H. Woodward: General Sciences Corporation, Laurel, Maryland; Robert A. Barnes: CHEMAL, Inc., Wallops Island, Virginia; Elaine R. Firestone: General Sciences Corporation, Laurel, Maryland.				
<b>12a. DISTRIBUTION/AVAILABILITY STATEMENT</b> Unclassified-Unlimited Subject Category 48 Report is available from the National Technical Information Service, U.S. Dept. of Commerce, 5285 Port Royal Road, Springfield, VA 22151; (703) 557-4650.			<b>12b. DISTRIBUTION CODE</b>	
<b>13. ABSTRACT (Maximum 200 words)</b> Post-launch stability monitoring of the Sea-viewing Wide Field-of-view Sensor (SeaWiFS) will include periodic sweeps of both an onboard solar diffuser plate and the moon. The diffuser views will provide short-term checks and the lunar views will monitor long-term trends in the instrument's radiometric stability. Models of the expected sensor response to these observations were created on the SeaWiFS computer at the National Aeronautics and Space Administration's (NASA) Goddard Space Flight Center (GSFC) using the Interactive Data Language (IDL) utility with a graphical user interface (GUI). The solar model uses the area of intersecting circles to simulate the ramping of sensor response while viewing the diffuser. This model is compared with preflight laboratory scans of the solar diffuser. The lunar model reads a high-resolution lunar image as input. The observations of the moon are simulated with a bright target recovery algorithm that includes ramping and ringing functions. Tests using the lunar model indicate that the integrated radiance of the entire lunar surface provides a more stable quantity than the mean of radiances from central ized pixels. The lunar model is compared to ground-based scans by the SeaWiFS instrument of a full moon in December 1992. Quality assurance and trend analyses routines for calibration and for telemetry data are also discussed.				
<b>14. SUBJECT TERMS</b> SeaWiFS, Oceanography, Modeling, Solar Observations, Lunar Observations, Calibration			<b>15. NUMBER OF PAGES</b> 26	
			<b>16. PRICE CODE</b>	
<b>17. SECURITY CLASSIFICATION OF REPORT</b> Unclassified	<b>18. SECURITY CLASSIFICATION OF THIS PAGE</b> Unclassified	<b>19. SECURITY CLASSIFICATION OF ABSTRACT</b> Unclassified	<b>20. LIMITATION OF ABSTRACT</b> Unlimited	